INVESTIGATION OF ECCENTRICALLY LOADED CIRCULAR CONCRETE-FILLED TUBULAR (CFT) STEEL COLUMNS BY FIBER STRESS ANALYSIS (FSA) METHOD

by

Oğuzhan Kaptanoğlu

B.S., Civil Engineering, Boğaziçi University, 2005

Submitted to the Institute for Graduate Studies in
Science and Engineering in partial fulfillment of
the requirements for the degree of
Master of Science

Graduate Program in Civil Engineering

Bogaziçi University

2008

INVESTIGATION OF ECCENTRICALLY LOADED
CIRCULAR CONCRETE-FILLED TUBULAR (CFT) STEEL COLUMNS
BY FIBER STRESS ANALYSIS (FSA) METHOD

APPROVED BY:

Prof. Cengiz Karakoç . . . . . .

(Thesis Supervisor)

Assoc. Prof. Orhun Köksal . . . . . .

Asst. Prof. Kutay Orakçal . . . . . .

DATE OF APPROVAL: 15.09.2008

To my hero, my father;

to my angels, my sisters, Figen and Miray...

ACKNOWLEDGEMENTS

Firstly, I would like to thank to my thesis supervisor, Professor Cengiz Karakoç, for spending his invaluable time, directing me towards different ways to investigate my thesis topic and sharing his great experience and vision, but most important showing his politeness and gentleness during my whole study.

I also would like to express my special thanks to the members of my thesis committee, Asst. Professor Kutay Orakçal for their assistance and advices to my thesis, helping me with patience and guiding when I could not exceed the handicaps of my research topic. Furthermore, Assoc. Prof. Orhun Köksal is one of the great contributors of this thesis study, who spent his time to trying different methods to complete my thesis study.

Lastly, I want to state that this thesis work was completed with the endless love, help, support and motivation of my father during my thesis work. This study could not be finished without him.

ABSTRACT

The composite columns also known by the name “Concrete Filled Tubular (CFT) Steel Columns” have been preferred increasingly in the construction of high-rise buildings, bridges, towers etc. in many countries in the world. Recently, a number of research papers have been published to investigate the behavior of these structural elements in literature. In this study, a computer program, which is based on an analysis method called as “Fiber Stress Analysis (FSA)”, was developed to understand the behavior of CFT steel columns. In this computer program, the entanglement of the FSA due to the discretization of the circular composite cross section was surpassed by introducing some geometric expressions. The required concrete and steel material models were adopted from Sakino [16] in order to calculate fiber stresses. In the FSA software, a number of iterative calculations are done by computer to satisfy equilibrium equations and get a series of moment vs. curvature points of any composite column. The verification of the FSA program is executed by comparing the test results of eccentrically loaded 18 circular CFT columns performed by Fujimoto [1]. At the end of this study, it is observed that the FSA method gives accurate results and it is a rapid solution technique in the analysis of circular CFT columns. It is also seen that the steel tube strength has a positive effect on the ductility of CFT column. On the contrary, the increase of concrete strength, axial load and diameter to thickness ratio reduces the ductility of composite column.

ÖZET

Kompozit kolonlar ya da diğer ismiyle "Betonla Doldurulmuş Çelik Tüp (CFT)" kolonlar yüksek yapılar, köprüler ve kule tipi gibi yapıların inşaatlarında dünyanın birçok ülkesinde çokça tercih edilmektedir. Son zamanlarda bu elemanların davranışlarını açığa çıkarmak amacıyla çok sayıda araştırma yazısı yayınlanmıştır. Bu tez çalışmasında, dairesel CFT kolonların moment-eğrilik diyagramlarını oluşturmak suretiyle, davranışlarını kavramak için, "Fiber Gerilme Analizi (FSA)" olarak bilinen bir analiz metodolojisine dayalı, bir bilgisayar yazılımı geliştirildi. Bu programda, FSA analizi için dairesel CFT kesitin fiberlere ayrılmasından kaynaklanan zorluklar, geometriye dayalı matematiksel formüllerin sunulmasıyla aşıldı. Fiberlerdeki gerilme değerlerinin hesaplanması için gereken beton ve çelik malzeme modelleri olarak, Sakino' nun önerdiği modeller kullanıldı. FSA programında, kompozit kolonun özellikleri girildikten sonra, denge denklemleri sağlanıncaya kadar bilgisayar tarafından çok sayıda iteratif hesaplama yapılmakta ve o kolon için bir dizi moment-eğrilik noktası elde edilmiş olunmaktadır. FSA programından elde edilen sonuçlar, Fujimoto' nun test ettiği 18 adet eksantrik yüke maruz dairesel CFT kolonun deney sonuçlarıyla kıyaslandı. Bu tez çalışması sonucunda, FSA metodunun dairesel CFT kolonların analizinde tutarlı ve doğru sonuçlar verdiğini ve aynı zamanda bu sonuçları da çok hızlı bir şekilde bulduğunu göstermiştir. Ayrıca, malzeme dayanımının artmasının sünekliliği arttırdığı doğrulandı. Buna karşılık, beton malzeme dayanımı, çap-kalınlık oranı ve eksenel yükteki artış ise düktiliteyi azaltmaktadır.

TABLE OF CONTENTS

LIST OF FIGURES

LIST OF TABLES

LIST OF SYMBOLS / ABBREVIATIONS

$A_c(i)$	Area of concrete element in i^{th} fiber
$A_s(i)$	Area of steel element in i^{th} fiber
b_c , b_s	Length of concrete and steel parts in the fiber
c	Distance between N.A. and compression side of the column
D	Diameter of CFT column
D_c	Diameter of concrete core, from center to inner circumference of tube section
$d\theta$	Unit rotation angle of member
E_c	Elastic modulus of unconfined concrete
E_s	Elastic modulus of steel
E_t	Inelastic modulus of steel
F_{int}	Internal force in CFT column
$F^{up}{}_c(i)$, $F^{down}{}_c(i)$	Load carried by concrete parts in upper and down i^{th} fibers, respectively
$F^{up}{}_s(i)$, $F^{down}{}_s(i)$	Load carried by steel parts in upper and down i^{th} fibers, respectively
i	Fiber index
k	Confinement coefficient, (taken as *4.1*)
K	Curvature of CFT section
k_e	An empirical value, taken as *23*
$m_{up}(i)$	Distance between midpoint of i^{th} fiber and N.A. of the CFT column
$m_{down}(i)$	Distance between midpoint of i^{th} fiber and N.A. of the CFT column
M	Internal moment at CFT column section
$M^{up}(i)$, $M^{down}(i)$	Moment carried by both concrete and steel in upper and down i^{th} fibers, respectively

n	Number of discretized fiber in a half portion of CFT column
N	Internal force on the CFT column
$p(i)$	Distance between midpoint of i^{th} fiber and center line of the CFT column
P	Load applied on the CFT column
$s(i)$	Distance between down edge of upper i^{th} fiber and center line of column
t	Thickness of steel tube section
t_f	Thickness of fiber
x	Distance between fiber midpoint and reference point
$\Delta\varepsilon$	Error margin
$\alpha_{in}(i)$	Inner angle calculated for i^{th} fiber
$\alpha_{out}(i)$	Outer angle calculated for i^{th} fiber
α_u, β_{uc}	Normalized hoop stress and axial stress in circular steel tube at ultimate load
γ_u	Strength reduction factor
ε	Strain of concrete and steel
ε_{co}	Strain at maximum strength of unconfined concrete, σ_c
ε_{cco}	Strain at maximum strength of confined concrete, σ_{ccB}
ε_{comp}	Strain at the compression side
$\varepsilon_{down}(i)$	Strain of i^{th} down fiber calculated at the midpoint of fiber
ε_{top}	Strain at the outer-most compression side or assumed strain
$\varepsilon_{up}(i)$	Strain of i^{th} up fiber calculated at the midpoint of fiber
ε_s	Strain at maximum strength of steel, σ_s
ε_{sc}, ε_{st}	Strain at maximum strength of steel in the case of compression and tension, respectively
ε_{su}	Strain at tensile strength, σ_{st}
ρ	Radius of curvature

σ	Stress of concrete and steel
σ_c	Cylinder strength of concrete
σ_c , σ_s	Stress of concrete and steel parts in the fiber
σ_{ccB}	Strength of confined concrete
σ_{cp}	Compressive strength of plain concrete
σ_r	Hoop stress on the steel tube
σ_{re}	Confining stress on the concrete provided by steel section
σ_s	Yield strength of steel
$\sigma_{s\theta}$	Radial stress on the steel tube at the ultimate load
σ_{st}	Tensile stress of the steel tube
σ_{sz}	Axial stress on the steel tube at the ultimate load
$\sigma^{up}{}_c(i)$, $\sigma^{down}{}_c(i)$	Stress on concrete parts in upper and down i^{th} fibers, respectively
$\sigma^{up}{}_s(i)$, $\sigma^{down}{}_s(i)$	Stress on steel parts in upper and down i^{th} fibers, respectively
φ	Curvature of section

CFT	Concrete Filled Tubular
FEM	Finite Element Method
FSA	Fiber Stress Analysis

1. INTRODUCTION

1.1. Overview

In the past decades, Concrete-Filled Tubular (CFT) steel columns have been greatly popular in high-rise buildings, bridges and so forth. They are very useful structural members because of high load carrying capacity, resistance to local buckling, seismic forces and high ductility. They are comprised of a steel hollow section and in-fill concrete, as represented in Figure 1.1. In composite columns, the steel tube of column provides confinement so enhances the axial load capacity as well as the energy absorption capacity or ductility; and the concrete core ensures a restraining force for the steel tube against buckling. Moreover, steel tube also employs as a formwork, so reduces construction cost and speeds up the construction works. Because of these exclusive features of the CFT steel columns, they are still one of the most important research issues in civil engineering field, to deceive their behavior under different types of loading. According to many academic researches done, it is known that the geometrical parameters e.g. diameter – thickness ratio, steel tube shape, material properties [1] and axial load applied on the column [2] are the most important factors affecting response of these columns.

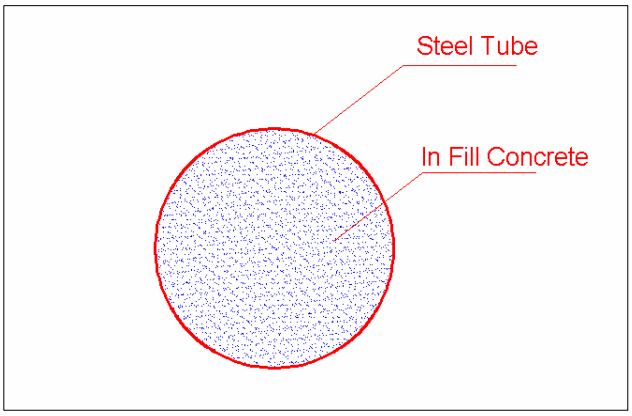

Figure 1.1 CFT cross section

In the scientific studies on the CFT columns, the main concentrated topics are condensed around the axial load capacity, ductility, bonding forces in concrete-steel tube interface and design criteria of CFT columns. Generally, in published experimental studies, the mathematical expressions for the material models, the effects of geometrical and physical parameters on the response or the stiffening scheme suggestions for composite columns are presented. On the other hand, in analytical studies about CFT columns, the analysis algorithms for nonlinearity issues, the modeling and simulation of CFT columns, the design equations of columns and their comparison with existed formula in design codes are mainly investigated. In recent works, correlated to development of computer programming and simulation technique, there has been a tendency to model composite columns by using computer program and match results with test data. Hence, the verification or the calibration of numerical expressions becomes possible, in addition to obtain a general solution for the CFT columns as well.

By utilizing computer, the CFT columns can be identified. Hence, the response of members under different type of loading, the material strength for steel and concrete and geometrical property, can be clarified without conducting experiments. The accuracy of the analysis results depends on the material models for steel and concrete, the computer algorithm, the increment ratios in the analysis and the assumptions accounted for the composite column analysis. In this study, an analysis algorithm was developed according to Fiber Stress Analysis (FSA) method, and a computer code was created in Matlab program. The required material models were obtained from a research paper, and applied to the FSA Matlab code. The material models include specific phenomena of concrete and steel such as concrete and steel behavior under multiaxial stress. All experimentally and analytically investigated specimens mentioned in this referred article (18-circular CFT steel column), were also analyzed with this new developed computer program based on the FSA technique. After that, their moments vs. curvature thrust diagrams were plotted. Then the results of the circular CFT steel specimens were compared with the test results and discussed.

1.2. Scope of Thesis

The aim of this thesis study is, to develop a computer program based on “Fiber Stress Analysis (FSA)” method in order to observe the behavior of the circular Concrete –Filled Tubular (CFT) steel columns under axial load and bending moment in combination; to verify the computer results with a set of experimentally tested specimens found from another research project; to discuss the effect of some geometric and physical parameters of composite column to the behavior.

2. LITERATURE SURVEY

In the formation stage of this thesis study, a comprehensive literature search was performed. More than 20 research papers were found and examined. While some of them constitute the foundation of the study in terms of FSA methodology, concrete and steel material behavior (e.g. confinement effect, friction and contact effect between tube and concrete), nonlinear material properties (e.g. Drucker-Prager Criterion, Von Misses Criterion); the remaining articles provided an overall contribution to CFT composite column behavior and analysis concept.

One of these research papers is "Behavior of Eccentrically Loaded Concrete-Filled Steel Tubular Columns" [3]. The main objectives of this research paper are to investigate the effect of higher material strengths on the flexural behavior of CFT columns and to create mathematical models for the steel tube and filled concrete materials. Adequate studies for the effects of the section shape, diameter, width-to-thickness ratio, the combination of strengths of the steel tube and filled concrete are included in the scope of this investigation. Based on the experimental results of 18 eccentric compression tests, an analytical model for the restoring force characteristics of the flexural behavior of CFT columns is proposed. The material models for concrete and steel tube are taken from Sakino's work. In this thesis study, the verification of the developed FSA program was conducted using the test results of 18 specimens revealed in this research article.

Secondly, "Nonlinear Analysis of Steel-Concrete Composite Structures-State of the art" [4] is another main resource for this thesis. In this study, the researchers compile many non-linear analysis techniques including fiber element analysis techniques in literature. The steel and concrete material models, fiber discretization techniques, section resultant presentation sorts are indicated extensively in this paper. Also a general information about the geometric nonlinearity, material nonlinearity, local buckling of steel, residual stress in steel tube, interface slip and contact forces between two materials are presented.

Another published work is “A distributed plasticity model for concrete-filled steel tube beam-columns with interlayer slip” [5]. A fiber-based distributed plasticity finite element formulation is suggested to perform three-dimensional monotonic analysis of square or rectangular concrete-filled steel tube (CFT) beam-columns. This stiffness-based beam-column element formulation comprehensively accounts for all significant geometric nonlinearity exhibited by CFT beam-columns as part of composite frame structures, and the steel and concrete constitutive models account for the significant inelastic phenomena, which are observed in the CFT column experiments. In addition, the finite element formulation accounts for the slip between the steel and concrete components of the CFT columns by incorporation of a nonlinear slip interface. This formulation is able to capture behavior ranging from the perfect bond to the immediate slip. The calibration and verification of the slip formulation are presented, and the finite element model is verified against experiments of CFT beam-columns subjected to monotonic loading. As a conclusion of these studies, it is expressed that the peak moment capacity is slightly affected by layer stiffness value, even if slip occurs in the composite column.

“Behavior of reinforced and concrete-encased composite columns subjected to biaxial bending and axial load” [6] which is one of the scarce studies conducted in Turkey about composite columns, is another important research report about CFT column behavior. An experimental investigation of the behavior of the reinforced concrete columns and a theoretical procedure for the analysis of both short and slender reinforced and the composite columns of arbitrarily shaped cross section subjected to biaxial bending and axial load are presented. In the proposed procedure, nonlinear stress–strain relations are assumed for concrete, reinforcing steel and structural steel materials. The compression zone of the concrete section and the entire section of the structural steel are divided into adequate number of segments in order to use various stress–strain models for the analysis. The slenderness effect of the member is taken into account by using the “Moment Magnification Method”. This study helps the generation of the compute algorithm for the developed FSA computer program in this thesis work.

“Finite element analysis of CFT columns subjected to an axial compressive force and bending moment in combination” [2] is a significant research project paper, which discusses the moment curvature relation of CFT columns by utilizing the concrete material

model proposed by Saenz. This paper includes an analytical work, which is the calibration of the concrete model using the test results of circular CFT columns. Six CFT steel composite columns are modeled in a finite element package program, ABAQUS, and then the concrete model is modified according to the test results. In conclusion, some equations for concrete material model attributed to the ratio of axial load to nominal load capacity are suggested. It is reported that the confining pressure provided by the steel tube increases with the increase of the axial load ratio on the column.

"Composite Action in Concrete –Filled Tubes" [7] is a research paper which investigates the bonding formation of CFT steel columns in the contact surface between steel tube and concrete core. An experimental work and a computer analysis are done to understand the phenomenon of the contact surface interaction of concrete and steel. It is shown that the shrinkage of concrete, which depends on the characteristics of the concrete, the diameter of the tube, and the surface condition at the inside of the tube, can be very detrimental to the bond stress capacity. The bond capacity is smaller in the tubes with large diameter and large d/t ratios. It is interrelated with the slip at the steel concrete interface. An exponential distribution of the bond stress is observed prior to slip, and a uniform distribution occurs after slip. An equation for the bond stress capacity at the interface surface is proposed in the conclusion of paper.

The study of "Representation of Concrete –Filled Steel Tube Cross Section Strength" [8] makes mention of the development of a polynomial equation to represent the three-dimensional (3D) cross-section strength, under axial load and biaxial bending of square or rectangular concrete-filled steel tube (CFT) beam-columns. The suggested expression is verified against the results of a detailed fiber analysis formulation, and against experimental tests of short, square CFT columns available in the literature. This CFT cross-section strength equation forms a compact expression of the failure surface of square or rectangular CFT columns having a wide range of cross-section dimensions and material strengths. Another application of the fiber resultant analysis is employed in this paper, so it contributes to the FSA computer program created in the thesis work.

In the research paper of “Nonlinear Analysis of In-Filled Steel-Concrete Composite Columns” [9], a method to predict the behavior of in-filled columns is presented. Moment-curvature-thrust relationships are found for column cross sections by using an iterative process. Stiffness based, nonlinear equilibrium equations resulting from geometric and material nonlinearities are solved by an incremental-iterative numerical scheme based on the generalized displacement control method. The accuracy of the proposed analytical method is established by comparing the numerical results with the corresponding experimental values. This paper includes significant information about the essentials of the FSA method, the assumptions that shall be considered in the analysis and the phases of lateral pressure formation around the infill concrete during the loading of column.

In the article of “Behavior of normal and high strength concrete-filled compact steel tube circular stub columns” [10] the behavior and design of axially loaded concrete-filled steel tube circular stub columns are presented. A finite element model is developed to carry out the analysis. Nonlinear material models for confined concrete and steel tubes are used. The column load carrying capacities and load–axial shortening curves are shown. The results obtained from the finite element analysis are verified against experimental results. A parametric study is conducted to investigate the effects of different concrete strengths and cross-section geometries on the strength and behavior of the concrete-filled compact steel tube circular stub columns.

“Nonlinear analysis of concrete-filled thin-walled steel box columns with local buckling effects” [11] is a useful research paper for the thesis study. The local buckling phenomenon for steel square and rectangular CFT columns are explained comprehensively, further it is stated that the circular CFT columns are robust against local buckling. The effects of local buckling are not considered in advanced analysis methods that lead to the overestimates of the ultimate loads of composite columns and frames. It is presented a nonlinear fiber element analysis method for predicting the ultimate strengths and behavior of short concrete filled thin-walled steel box columns with local buckling effects. The fiber element method considers nonlinear constitutive models for confined concrete and structural steel. Moreover, the equations for geometric imperfections and residual stresses of steel section are incorporated in the fiber element analysis program.

3. CONCRETE FILLED TUBULAR (CFT) COLUMNS

3.1. Specifications of CFT Steel Columns

Concrete Filled Tubular (CFT) steel columns are very tough structural members, which are used in high-rise buildings, bridges and so forth. The brittle concrete and ductile steel materials cooperate and a high performance structural member is obtained. However, the combination of these two different material makes CFT column behavior sophisticated. The behavior of circular CFT columns depends on some factors. These factors can be ranged as material strength of steel and concrete, confinement effect, local buckling of steel tube and interface condition between steel and concrete.

3.1.1. Material Strength

The main function of the concrete in CFT composite columns is to increase the load carrying capacity and to counteract the failure of steel from local buckling. In the case of circular CFT columns, the ultimate compressive strength of concrete is increased due to lateral pressure exerted to its transverse surface by steel tube section. Hence, the concrete in the tube is stressed triaxially; which can be explained by Drucker-Prager yielding criterion. This criterion is most often used for concrete where both normal and shear stresses can determine failure. The criterion is a pressure-dependent model for determining whether a concrete has failed or undergone plastic yielding [12]. Although concrete strength is improved by tube confinement, the increase of cylindrical concrete strength reduces the ductility of member. Therefore, attention is necessary for the concrete strength in CFT columns [1]. The axial tensile strength of a CFT column may be approximated by assuming that only the strength of the steel tube contributes to the load resistance. Because, in the case of tensile loading of a CFT columns, the concrete cracks at the early stages of loading, so the steel tube and concrete core barely interact.

The CFT composite column behavior is notably affected by steel grade. The higher strength and thicker steel tubes give better overall behavior of the beam column. The

ductility becomes larger as the steel strength becomes higher [13]. As in the case of concrete subjected to multiaxial stress, there is biaxial stress steel state in the steel tube. The steel tube of a circular CFT column resists the axial stress σ_v on the one hand, and is exposured to a horizontal pressure, σ_h through its axis of plane, on the other hand as shown in Figure 3.1. This action leads to steel section yield stress, σ_s, to reach a higher stress value σ_{st} in the case of an axial tensile load on the steel tube. On the contrary, steel tube yield stress, σ_s, falls down to a lower stress value σ_{sc} in the case of an axial compressive load on the steel tube. This phenomenon is known as "Von Misses Yield Criterion". Another concept of steel materials, "strain hardening" may be accounted for fiber stress analysis.

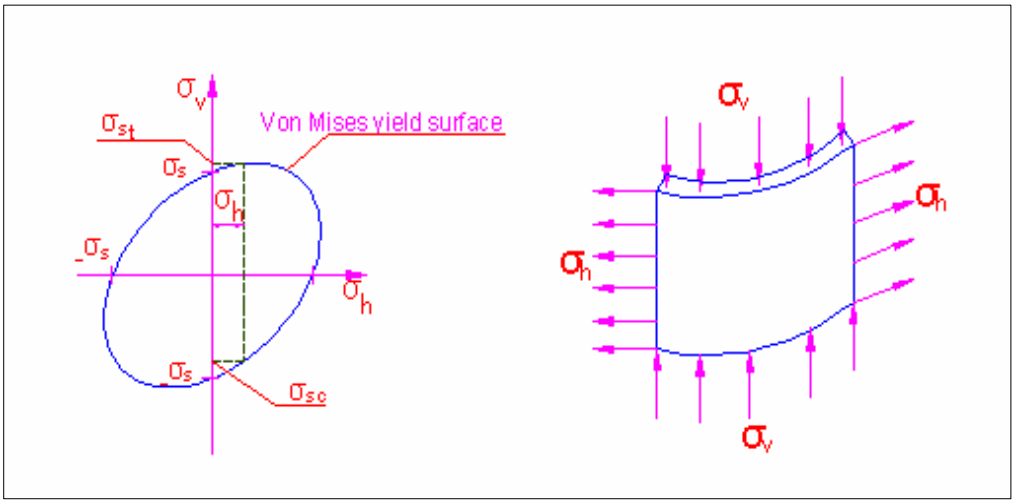

Figure 3.1. Von Misses yield criterion

3.1.2. Diameter to Thickness (D/t) Ratio

The ratio of diameter to thickness (D/t) of the steel tube section is a significant parameter for composite columns. Concrete-filled steel tube circular columns with a high value of the D/t ratio provide inadequate confinement for the concrete. On the other hand, concrete-filled steel tube circular columns with a small value of the D/t ratio provide remarkable confinement for the concrete [14].

3.1.3. Confinement Effect

Due to the interaction between the steel and the concrete in a circular CFT column, a triaxial stress state is developed in concrete core, which corresponds to the "confinement of concrete". When a CFT column is subjected to axial load as shown in Figure 3.2, the Poisson's ratio for concrete is lower than that for steel and the steel tube has no restraining effect on the concrete core, in the early stages of loading. As the longitudinal strain increases, Poisson's ratio of concrete- which is 0.15–0.2 in elastic range, can remarkably increase in the equitriaxial compressive regime. Therefore, the lateral expansion of unconfined concrete gradually becomes greater than that of steel. A radial pressure develops at the steel–concrete interface thereby restraining the concrete core, σ_{re} and setting up a hoop tension in the tube, σ_{θ}. At this stage, the concrete core is stressed triaxially and the steel tube biaxially [9]. As a reason for the confinement, the concrete shows greatly increased maximum compressive strength, increased stiffness, and extended strain at which the peak stress is reached. The confined concrete can sustain large deformation without substantial reduction of the load-bearing capacity and fails gradually in a ductile way [14].

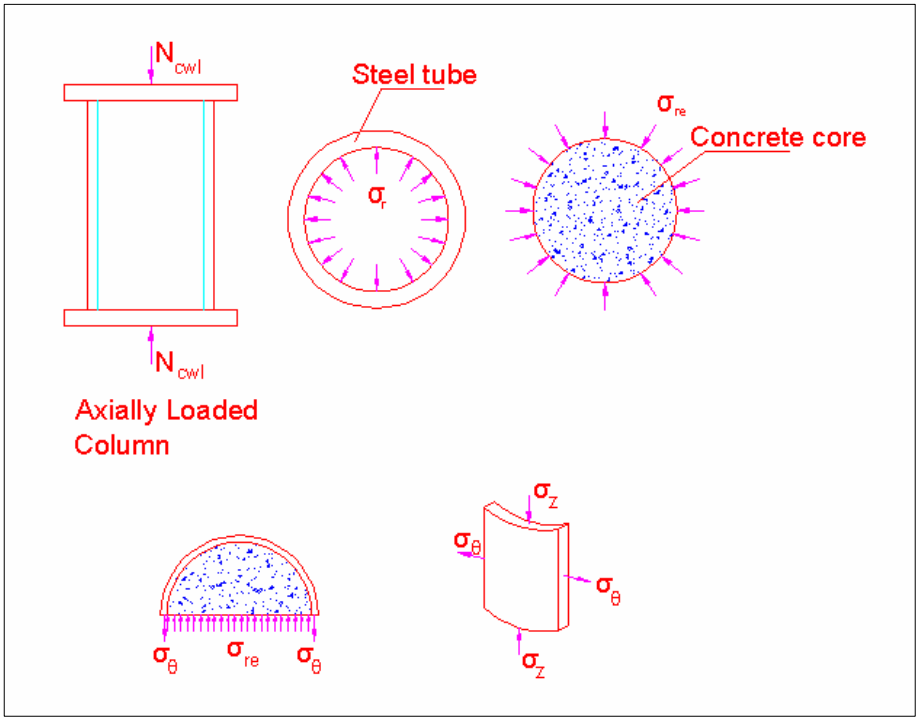

Figure 3.2. Stresses on the concrete core and steel tube of circular CFT steel column, under axial load

3.1.4. Local Buckling

In engineering, buckling is a failure mode characterized by a sudden failure of a structural member subjected to high compressive stresses, where the actual compressive stresses at failure are greater than the ultimate compressive stresses that the material is capable of withstanding. This mode of failure is also described as failure due to elastic instability. In circular CFT columns, the column shape has an important effect on column buckling resistance. It has been experienced from the past studies that circular tubes are more resistant than square columns, due to its radial geometric shape. Another factor in the local buckling event is the tube thickness. Local buckling generally occurs at lower deformations as the diameter or width to thickness ratio increases. The strength of the square columns reduces as the ratio increases. This fact causes local buckling and fracture of the steel tube to occur at early deformation stages. However, the circular CFT columns have good resistance to local buckling [5].

3.1.5. Concrete-Steel Bonding

In order for an effective performance of composite columns, strong bonding forces between concrete core and steel inner surface are required. The bond transfer between the steel tube and the concrete fill depends on the radial displacements due to the pressure of the wet concrete on the shell and the shrinkage of the concrete core, together with the rugosity (or internal surface irregularities) of the interior surface of the tube. The interlock between concrete and steel is greatly affected by tube diameter. Large d/t ratios are also significant; tubes with large d/t ratios have much smaller radial stiffness than tubes with lower d/t values. As a result, tubes with large d/t ratios distort easily and develop smaller bond resistances due to the interlock effect. The bond stress in the contact surface is concentrated along a region near the load applied to column. If the slip between steel and concrete under interface shear is prevented, the bond stress demand is completed within a length of approximately d/2 with an exponential distribution along the interface. The transfer length is longer than d/2 with low d/t ratio CFT columns and shorter than d/2 with large d/t ratios. If slip occurs at the interface, the bond stress is approximately uniform over the slipped region [7]. In CFT composite columns, greater d/t ratio decreases contact force, and ductility as well.

In the construction of CFT columns, some methods exist in order to increase bond stress capacity, called as “stiffening”. It is generally constructed by welding steel bars to the inner face of steel tube section. The provided contact force depends on the arrangement, diameter, and spacing of tie bars [15]. Another solution to CFT columns is “Novel” sections. In this type of composite columns, internal longitudinal symmetric stiffeners are welded to the inside surface of steel wall throughout the length of column. These sections can be produced by welding at the workshops of construction sites with special arrangements and careful preparations. In novel CFT columns, load transferring can be provided appropriately due to the increase in the contact surface between steel and concrete. Using internal longitudinal symmetric stiffeners causes the contact surface between steel and concrete to be increased, hence, the effects of creep and shrinkage decrease considerably [16].

The concrete-steel interface relationship is a sophisticated topic, yet reducing the initial slip layer stiffness by some magnitude reduces the initial flexural stiffness of the members by a negligible amount, and it does not noticeably change the ultimate moment strength of these members. In general, the magnitude of strength, stiffness and deformation of the members changed very little. It can be concluded that, even for the more extreme conditions (e.g. wind and cyclic forces in a braced frame), the slip is seen to have a little effect on the global behavior of a composite CFT frame, or on the strength achieved by a CFT member subjected to flexure[5].

Figure 3.3. A novel CFT steel column

3.2. Analysis Methods of CFT Columns

The response of CFT columns can be observed with different analysis methods in literature. There are several numerical methods to analyze composite members such as Finite Element Method (FEM), and Fiber Stress Analysis (FSA) Methods.

One of the methods mentioned above is the “Finite Element Method” which can be regarded as a natural extension of the matrix methods of structural analysis. It can accommodate complex and difficult problems such as nonhomogenity, nonlinear stress–strain behavior, and complicated boundary conditions. The finite element method is applicable to a wide range of boundary value problems in engineering. The method can be applied to the solution of plane stress problems and extended subsequently to the solution of plates, shells, and axisymmetric solids. The finite element method is based on the representation of a body or a structure by an assemblage of subdivisions called finite elements. These elements are considered to be connected at nodes. Displacement functions are chosen to approximate the variation of displacements over each finite element. Polynomial functions are commonly employed to approximate these displacements. Equilibrium equations for each element are obtained by means of the principle of minimum potential energy. These equations are formulated for the entire body by combining the equations for the individual elements so that the continuity of displacements is preserved at the nodes. The resulting equations are solved satisfying the boundary conditions in order to obtain the unknown displacements. The entire procedure of the finite element method involves the following steps [17]:

- The given body is subdivided into an equivalent system of finite elements.
- A suitable displacement function is chosen.
- The element stiffness matrix is derived using a variation principle of mechanics, such as the principle of minimum potential energy.
- The global stiffness matrix for the entire body is formulated.
- The algebraic equations thus obtained are solved to determine unknown displacements.
- The element strains and stresses are computed from the nodal displacements.

In the analysis of CFT columns with the FEM, the interaction between steel tube and filling concrete can be taken into account by using “spring elements”, hence a more realistic behavior is observed. Generally, the friction coefficient is accepted as 0.25. By considering contact stiffness, it is possible to examine the effect of slip and friction between layers on the load deformation behavior. The stresses on the CFT column are generally presented as stress resultant gradient because of using 3D solid elements along the element length. Therefore, the analysis of circular CFT columns with FEM takes longer time.

Another method, the “Fiber Stress Analysis” (FSA), which will be used in this thesis study, is a technique in which the CFT section is subdivided into an amount of fibers -not necessarily of equal area. In order to determine the section response of a member by FSA, each fiber in the CFT section is assigned to concrete or structural steel material properties in the column after discretization. Making use of the ‘‘plane sections remain plane’’ assumption, the elongation/shortening will be a linear function, for a trial strain value at the outer most fiber. By geometry, the strain can be found at the midpoint of each fiber. Owing to relevant constitutive models, the fiber stresses are calculated from these fiber strains. The method followed when finding the fiber strains as the load history on the section progresses is, to follow the migration of the section neutral axis during the load history. The stress resultants of the circular CFT member are calculated at the centroid of each segment. The stresses are integrated over the cross-sectional area to obtain the fiber resultants such as force and moment. In this way, the summation of fiber element forces allows the determination of internal force, while the summation of fiber element moments is used to determine the internal moment of the CFT steel column, as expressed in the following equations:

$$N = \int_{x=0}^{x=D} [b_s(x)\sigma_s(x) + b_c(x)\sigma_c(x)]dx \tag{3.1}$$

$$M = \int_{x=0}^{x=D} (x-c)[b_s(x)\sigma_s(x) + b_c(x)\sigma_c(x)]dx \tag{3.2}$$

where;

N : Internal force

M : Internal moment

D : Diameter of CFT column

b_c, b_s : Length of concrete and steel parts in the fiber, respectively

σ_c, σ_s : Stress of concrete and steel parts in the fiber, respectively

c : Distance between N.A. and compression side of the column

x : Distance between fiber midpoint and reference point

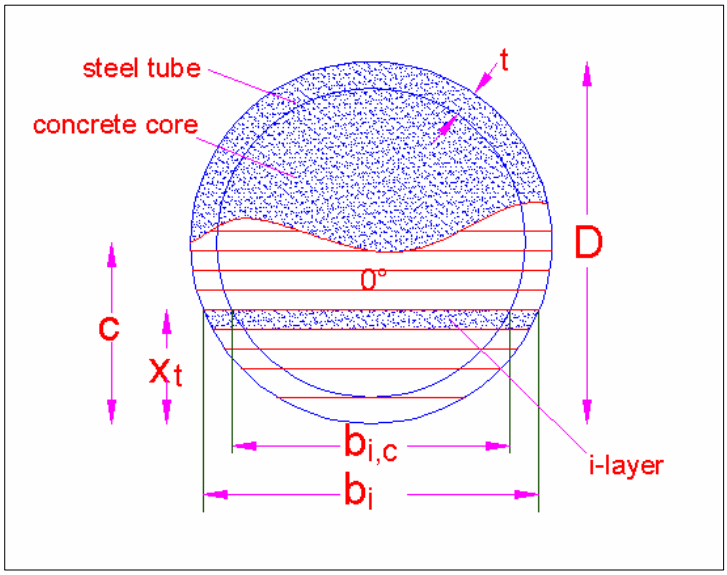

Figure 3.4. A general fiber discretization of CFT column

The fiber stress model generally makes use of a number of assumptions:

- Plane sections remain plane after bending. It is generally accepted that this assumption is reasonably accurate even within the inelastic range.

- Shear and torsion stresses are neglected. For this reason, the fiber method is generally used for the analysis of flexure-dominated members, where the Euler-Bernoulli beam theory can be reasonably applied.
- Although constitutive relations are typically defined as uniaxial, multiaxial stress states -such as those due to confinement effects or concrete constraint to steel tube- can be included by increasing the concrete strength and by modifying the concrete post peak response.
- Concrete cracking is generally accounted for. However, the cracking is considered smeared and normal to the member axis because of the plane section assumption.
- Local buckling of the steel components and initial stresses resulting from either erection loads or thermal residual effects can be included.

In the case of using numerical solution methods, the material models for concrete and steel identify the element response. In order to predict the moment-curvature or axial load-strain relationships of CFT columns, a stress–strain model for confined concrete and steel hollow section are required. These material models reflect the multiaxial behavior of both steel and concrete because of the steel tube confinement effect and infill concrete restraining effect. The confinement provided by the steel tube to the CFT beam-column leads to the increase of the ultimate compressive strength of infill concrete and the improvement for the post-peak behavior of composite columns. The stress-strain model for steel tube utilized in the fiber section analysis is a biaxial stress-strain relationship, and based on “Von Misses Yield Criterion”. The strain-hardening rule is usually accounted. Even though fiber analysis requires only uniaxial constitutive relationships, the response of steel in composite structures is the result of the complex multiaxial effects that include local buckling and residual stresses due to cold-forming and welding. These two events occurred in composite columns may be critical in square CFT columns rather than circular columns, which are classified as the “steel plate” structures.

The local buckling failure for CFT columns can be incorporated either by assuming a fixed effective width or by degrading the structural properties of the steel elements that reach a critical buckling stress in some researches. It is a fact that, local buckling is a

crucial phenomenon for square CFT columns but circular CFT columns are strong against local buckling. It can be asserted that not only circular CFT columns but also thick plate box CFT columns have also good resistance to buckling failure [10]. Therefore, the local buckling effect is disregarded because it is assumed that CFT columns will not suffer from the buckling stress in this study. Yet, the slenderness effect can be included in the FSA by using "Moment Modification Factor" [6], in which a lower peak moment capacity is obtained for CFT columns.

"Fiber Stress Analysis" is smarter and faster solution technique, compared to finite element analysis. If the section is discretized frequent and the increment values are selected small enough, the accuracy of analysis results will increase. Another factor for the reliability of the FSA is the selection of proper material stress-strain relationship for the analysis.

3.3. Moment-Curvature (M-φ) Relationship for CFT Columns

The moment vs. curvature diagrams are good indicators to determine the load vs. deformation behavior of structural members by using nonlinear material stress-strain relationships. In the case of an eccentrically loaded circular CFT column, there exist an extreme compression fiber strain and a section curvature at which the internal force is in equilibrium with the applied axial load. A unique bending moment can be calculated at this section curvature from the stress distribution. The extreme concrete compression strain and the section neutral axis position can be iterated until a range of moment-curvature values are obtained providing that the equilibrium equation is satisfied. Plotting these moment and curvature values constitutes the desired diagram [18]. Thus, instead of any experimental work, the behavior of CFT columns can be investigated analytically. The area under the curve gives information about the ductility of any column. The reliability of moment-curvature diagram is, however, associated to the accuracy of material model [19].

The term "curvature" is the unit rotation angle of member undergoing flexural bending. It can be expressed by utilizing either the difference between the rotation angle of

two section sliced over the column or the unit deformation on the cross section, as shown in Figure 3.5.

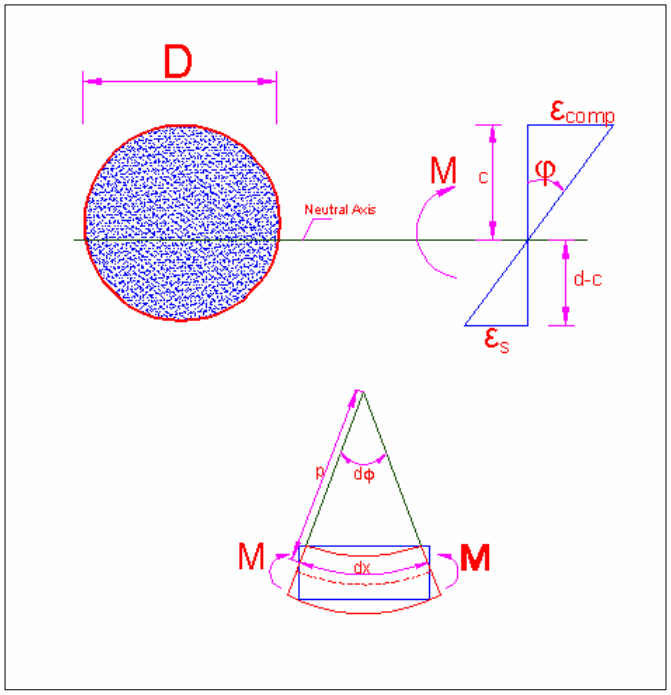

Figure 3.5. The moment and curvature of a circular CFT column

$$\varphi = \frac{1}{\rho} = \frac{d\theta}{dx} = \frac{d^2 y}{dx^2} \tag{3.3}$$

$$\varphi = \frac{\varepsilon_{comp}}{c} \tag{3.4}$$

where;

$\boldsymbol{\varphi}$: Curvature of section

$\boldsymbol{\rho}$: Radius of curvature

$\boldsymbol{d\theta}$: Unit rotation angle of member

$\boldsymbol{\varepsilon_{comp}}$: Strain at the compression side

$\boldsymbol{c}$: Distance between N.A. and compression side of the column

The shape of moment-curvature diagram gives significant data about the energy absorption capacity of columns. The moment-curvature (M - φ) curves can be divided into three regions based on calculated values of M and φ:

1) Elastic region, *A*
2) Elasto- plastic region, *B*
3) Plastic region, *C* [20].

In Figure 3.5, a sample moment curvature diagram is presented. In region A, the concrete and steel materials have elastic behavior. In this region, the concrete cracking occurs due to tensile stresses. As the moment increases, the curvature of column also increases but the steel tube initializes yielding due to the rise of the outermost fiber strain value. Not only steel tube, but also infill concrete strength turns to a slower increase rate corresponding to strain increase rate in this stage, due to the initial concrete crushing. This leads to the decrease of the moment increase ratio; however, the curvature of column continues increasing. This is shown as region B, which is called as "Elasto-Plastic" behavior. If the deformation on the column progresses, the member passes to the region C, then steel tube absolutely yields. The moment carried on the column changes with respect to the concrete behavior. The ductility provided by the steel tube determines the slope of moment-curvature line. The more the lateral pressure on the concrete core exists, in other words confinement; the less column moment carrying capacity deteriorates. During the

increase of moment on the section, the position of neutral axis migrates to the compression side of the CFT column.

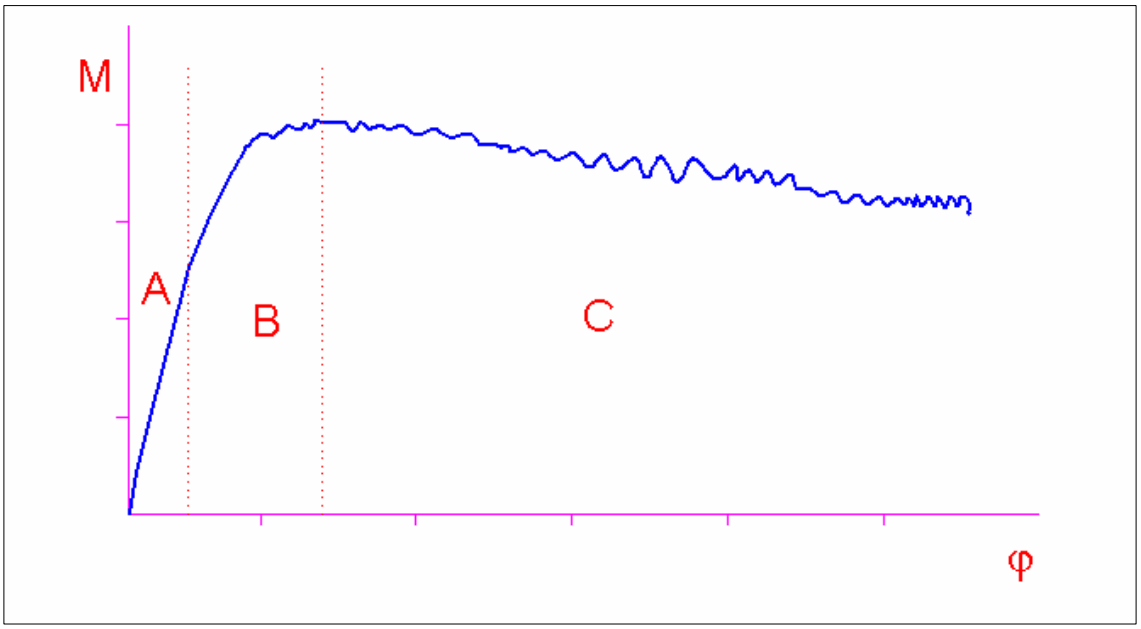

Figure 3.6. A representation moment vs. curvature graph of a circular CFT steel column

4. FIBER STRESS ANALYSIS (FSA) METHOD

4.1. Overview

In this study, the behavior of circular CFT columns is aimed to be examined by "Fiber Stress Analysis (FSA)". The FSA is an iterative process and basically comprised of,

- division of circular CFT steel column section into fibers,
- calculation of fiber area, distance between midpoint of fiber to the neutral axis and central line, as a function,
- calculation of strain of each fiber according to the position of neutral axis and outermost strain,
- determination of stress values of steel and concrete from concrete and steel uniaxial material models at the midpoint of fibers,
- calculation of internal force and moment contribution of each fiber respectively,
- summation of overall contributions of fibers,
- checking whether the equilibrium equation is satisfied or not.

In FSA, there are some assumptions specified for this thesis research as,

- plane sections remain plane after bending,
- there exists "Perfect Bonding" (no slippage) between in-fill concrete and steel tube,
- concrete tensile strength is not considered,
- local buckling of the steel tube is neglected.

The fiber analysis of the CFT columns is conducted by writing a computer program in MATLAB. The computer gives an amount of moment and curvature points of any circular CFT section whose geometric, physical, material properties and exerted load on it

are inputted to program by user. After entering these values to the program, iterations start for the outermost strain of compression side and the neutral axis (N.A.) position values**.** At first, a small starting strain value is accepted as a trial. Then the N.A. position shifts with a specified increment value. This increment value should be selected small enough to find moment vs. curvature points more accurately. It has an important role on the accuracy of the results. At each N.A. position, an axial load and moment value are found after the overall integration of the fiber forces. These values are considered as the axial load and the moment response of the section for that NA position and strain against the external load exerted to the CFT. When the difference between the axial load and fiber force summation is smaller than an acceptable error, the equilibrium equation is assumed to be satisfied. The overall moment on the section is the moment carried by the section at those trial values of the N.A. location and strain. In addition, the curvature of CFT column is calculated from those N.A and strain values. If the equilibrium equation is not satisfied, N.A. moves with a small value towards tension side of CFT column and all calculations are repeated. These computations continue until internal and external loads are approximately equal. This process is repeated for many arbitrary strain assumptions. Consequently, for each trial strain value of the compression side of column, a moment and curvature couple is obtained. Plotting these data in a graph constitutes the moment curvature diagram of that column.

4.2. Section Discretization

The half of the circular CFT column section is divided into 10 fibers, which are parallel to the neutral axis of section. In order to shorten the analysis duration, only one-half of the section is divided into fibers because the section is circular and it is symmetric with respect to both axes, as shown in Figure 4.1. As a result, the calculated fiber area at one side of section is used for the other side of the section. However, the distances to N.A. are different which are required to calculate the strain and the moment of the CFT section. In order to prevent singularity during the computer calculations, the thickness of fiber must be greater than tube thickness. To find the section capacities, the load and moment values of each fiber are summed from the first fiber to the last fiber by an iterative process.

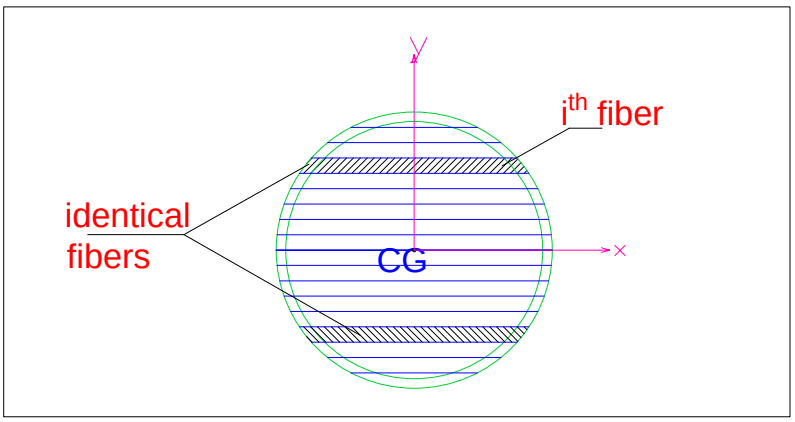

Figure 4.1. Section discretization of circular CFT section for FSA.

4.3. Fiber Formulations

In order to perform FSA, some geometrical properties must be established as mathematical expressions. The symmetry of circular CFT steel column is utilized to shorten analysis duration, so only one portion is discretized into fibers. As shown in Figure 4.2, the fibers, which are far from the centre line with the same distance, are identical. Their areas and distances to the centerline of the column section are all same. The CFT column is circular therefore; each concrete and steel fiber has different area unlike rectangular or square composite columns. This case leads to define new parameters to perform FSA calculations. The first parameter is the distance between down edge of fiber and centre line of column, *s*,:

$$s(i) = \sum_{1}^{i-1} s(i) - \frac{t_f}{2} \tag{4.1}$$

where;

i : Fiber index

s(i) *:* Distance between down edge of upper fiber and centre line of column

t_f : Thickness of fiber

The angles α_{IN} and α_{OUT} are defined in Figure 4.2. They can be expressed as;

$$\alpha_{IN}(i) = arccos(\frac{s(i)}{r}) \tag{4.2}$$

$$\alpha_{OUT}(i) = arccos(\frac{s(i)}{R}) \tag{4.3}$$

where;

$\alpha_{in}(i)$: Inner angle calculated for ith fiber

$\alpha_{out}(i)$: Outer angle calculated for ith fiber

Area of the fiber can be found in such a way that;

$$A_c(i) = \frac{2\alpha_{in}(i)\pi r^2}{360} - \frac{1}{2}r^2 \sin(2\alpha_{in}(i)) - \sum_{i=1}^{i-1} A_c(i) \tag{4.4}$$

$$A_s(i) = \frac{2\alpha_{out}(i)\pi r^2}{360} - \frac{1}{2}r^2 \sin(2\alpha_{out}(i)) - \left[\sum_{i=1}^{i} A_c(i) + \sum_{i=1}^{i-1} A_s(i)\right] \tag{4.5}$$

where;

$A_c(i)$: Area of concrete element in i^{th} fiber

$A_s(i)$: Area of steel element in i^{th} fiber

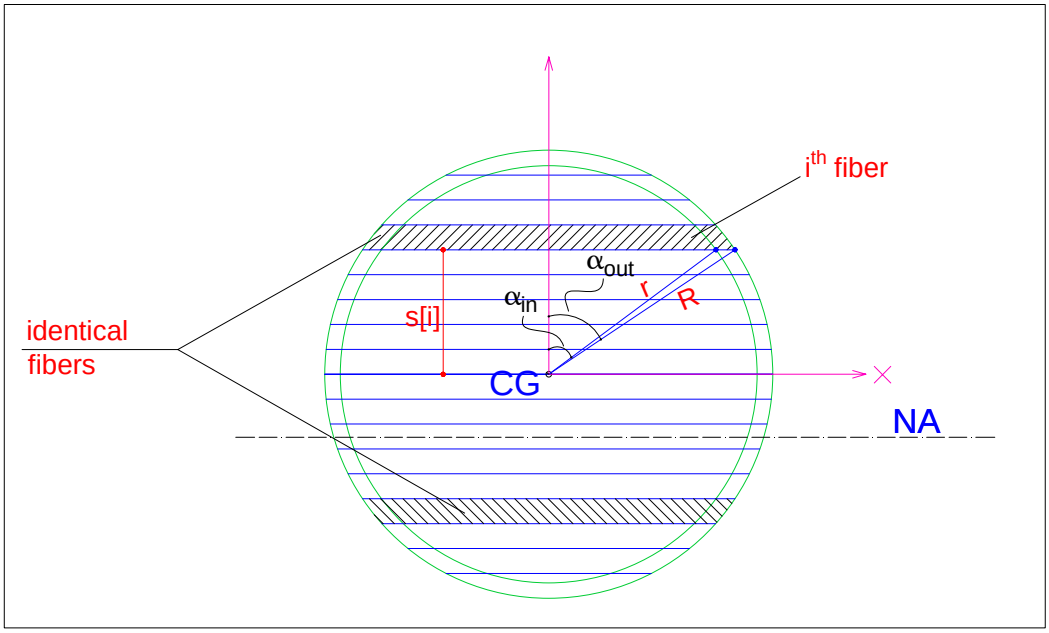

Figure 4.2. Required geometrical parameters for FSA calculations(1).

The strain of each fiber is calculated with respect to the center of the fiber. In order to find the fiber strain, firstly the distance between the center of fiber and the centerline of the column section; *p* and the distance between center of fiber and neutral axis; *m* must be stated. These terms are shown in Figure 4.3. The fiber strain has to be found for both up and down identical fibers separately, so do *m* value, which are;

$$p(i) = s(i) + \frac{t_f}{2} \tag{4.6}$$

$$m_{up}(i) = p(i) - c \tag{4.7}$$

$$m_{down}(i) = -p(i) - c \tag{4.8}$$

where;

p(i) : Distance between midpoint of i^{th} fiber and center line of the CFT column

c : Distance between position of N.A. and center line of the CFT column

$m_{up}(i)$: Distance between midpoint of i^{th} fiber and N.A. of the CFT column

$m_{down}(i)$: Distance between midpoint of i^{th} fiber and N.A. of the CFT column

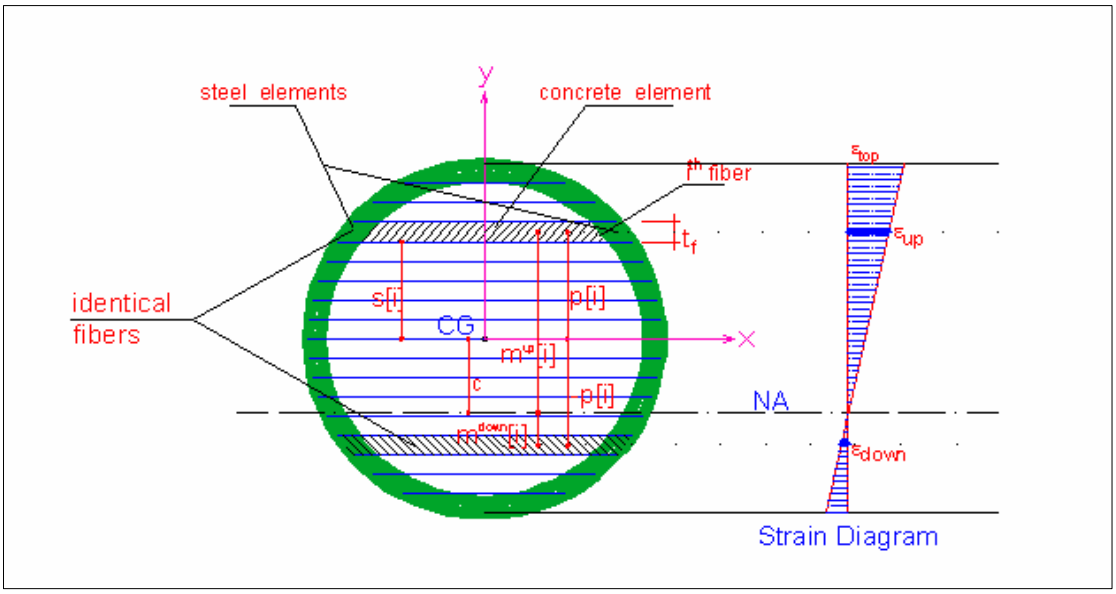

Figure 4.3. Required geometrical parameters for FSA calculations(2).

After that, the strain for up and bottom fiber values can be formulated separately as mathematical functions in the following equations:

$$\varepsilon_{up}(i) = \left(\frac{m_{up}(i)}{R - c} \right) \varepsilon_{top} \tag{4.9}$$

$$\varepsilon_{down}(i) = \left(\frac{m_{down}(i)}{R-c}\right)\varepsilon_{top} \tag{4.10}$$

where;

$\varepsilon_{up}(i)$: Strain of i[th] up fiber calculated at the midpoint of fiber

$\varepsilon_{down}(i)$: Strain of i[th] down fiber calculated at the midpoint of fiber

ε_{top} : Strain at the outer-most compression side or assumed strain

The strain values obtained from these equations for the upper and down identical fibers are used to find the upper and down fiber stresses for concrete and steel parts based on the material models. The force resultant for the down fibers for steel and concrete will be;

$$F_c^{down}(i) = A_c(i).\sigma_c^{down}(i) \tag{4.11}$$

$$F_s^{down}(i) = A_s(i).\sigma_s^{down}(i) \tag{4.12}$$

For upper fiber;

$$F_c^{up}(i) = A_c(i).\sigma_c^{up}(i) \tag{4.13}$$

$$F_s^{up}(i) = A_s(i).\sigma_s^{up}(i) \tag{4.14}$$

where;

$\sigma^{up}{}_c(i)$, $\sigma^{down}{}_c(i)$: Stress on concrete parts in upper and down i[th] fibers, respectively

$\sigma^{up}{}_s(i)$, $\sigma^{down}{}_s(i)$: Stress on steel parts in upper and down i[th] fibers, respectively

$F^{up}_{c}(i)$, $F^{down}_{c}(i)$: Load carried by concrete parts in upper and down i^{th} fibers, respectively

$F^{up}_{s}(i)$, $F^{down}_{s}(i)$: Load carried by steel parts in upper and down i^{th} fibers, respectively

The total internal load, F_{int}, on the circular CFT column equals the individual contribution of fibers particularly;

$$F_{int} = \sum_{1}^{n} \left[F_c^{up}(i) + F_s^{up}(i) + F_c^{down}(i) + F_s^{down}(i) \right] \tag{4.15}$$

$$\left| P - F_{int} \right| \leq \Delta\varepsilon \tag{4.16}$$

where;

n : Number of discretized fiber in half portion of CFT column

F_{int} : Internal force in CFT column

$\Delta\varepsilon$: Error margin

P : Load applied on the CFT column

As seen in eq. (4.16), if the difference between the calculated internal force and the external load on the CFT column is smaller than an acceptable margin, the system forces are assumed to be in equilibrium for that selected compression strain value and N.A. position. Then, the internal moment and the curvature stem from this moment will be;

$$M_{up}(i) = \left[F_c^{up}(i) + F_s^{up}(i) \right] m_{up}(i) \tag{4.17}$$

$$M_{down}(i) = \left[F_c^{down}(i) + F_s^{down}(i)\right] m_{down}(i) \tag{4.18}$$

$$M = \sum_{i=1}^{n} \left[M_{down}(i) + M_{up}(i)\right] \tag{4.19}$$

$$K = \frac{\varepsilon_{top}}{c} \tag{4.20}$$

where;

$M^{up}(i)$, $M^{down}(i)$: Moment carried by both concrete and steel in upper and down i^{th} fibers, respectively

K : Curvature of CFT column

4.4. Computer Algorithm

The calculation process or flowchart of FSA is shown in Figure 4.4. Based on this structure, a computer program code is written in Matlab. The code comprises some *for* and *if* loops; and some functions. This Matlab code is presented in Appendix A. The developed FSA program gives the moment resultant and the curvature of circular CFT column for each trial strain, ε, and N.A. position, c, values which satisfy the equilibrium equation, after entering inputs for the material properties and the geometric properties of any circular CFT column. The range for strain value, ε, is between 0.0001 and 0.1 with 0.0005 increment. Additionally, the neutral axis, c, will shift in an interval between 0.5 times R and $-R$ with -1 mm change. In each trial of c and ε, the program controls the eccentric load with the internal force, whether or not the difference, is small than 0.0001. The values of ε and c can be changed in order to obtain more moment vs. curvature points or to solve convergence problem before starting the FSA. As a result, when the program ends, a

number of moment and corresponding curvature points for every stage of ε and c value are obtained. The sign convention for the analysis results is so that the compression strains, stresses, forces and counter-clockwise moments are positive. These outputs are recorded by program and then converted into the moment –curvature graphics by using MS EXCEL.

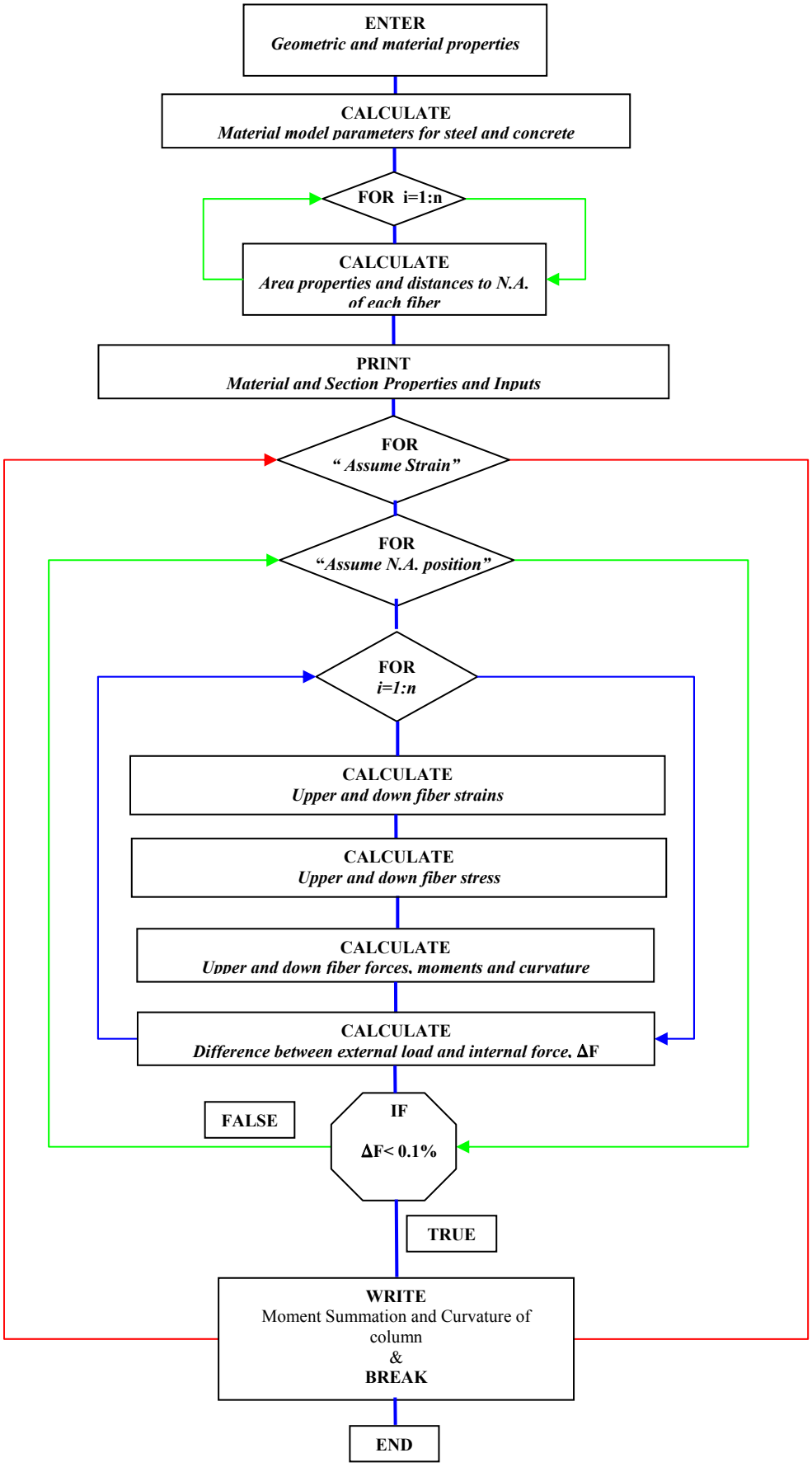

Figure 4.4. Flow chart for FSA Matlab code

5. MATERIAL MODELS

In order to examine the behavior of circular CFT columns by fiber section analysis, the stress–strain models for concrete and steel material that are developed for columns under eccentric loading are necessary. In this study, a concrete model developed for the CFT column- in fill concrete under axial load and uniaxial bending by *Sakino* [1] is used. For the steel tube of column, a bilinear steel model is used considering strain hardening phenomenon. Then, these models are assigned to steel and concrete parts of the fiber elements respectively.

5.1. Concrete Model

The Sakino's uniaxial concrete model used in this study takes into account the confining effects of the circular steel tubes, which ensures the increase in the concrete compressive strength and the improvement in the behavior after attaining maximum strength. The confined concrete response is affected by diameter, thickness, and material strengths. Here, the tensile strength of the concrete is ignored. The stress of concrete under compression is defined as;

$$\sigma = \frac{V\left(\frac{\varepsilon}{\varepsilon_{cco}}\right) + (W-1)\left(\frac{\varepsilon}{\varepsilon_{cco}}\right)^2}{1 + (V-2)\left(\frac{\varepsilon}{\varepsilon_{cco}}\right) + W\left(\frac{\varepsilon}{\varepsilon_{cco}}\right)^2}\sigma_{ccB} \tag{5.1}$$

where;

σ : Stress of concrete

σ_{ccB} : Strength of confined concrete

ε : Strain of concrete

ε_{cco} : Strain at maximum strength of confined concrete, σ_{ccB}

The terms V and W are defined in the following equations. Firstly, in this model, the scale effect on the concrete strength is considered by an equation, which is obtained by curve fitting the test results. The scaling coefficient, γ_u, and compressive strength of plain concrete, σ_{cp}, are;

$$\gamma_u = 1.67 D_c^{-0.112} \tag{5.2}$$

$$\sigma_{cp} = \gamma_u \sigma_c \tag{5.3}$$

where;

γ_u : Strength reduction factor

D_c : Diameter of concrete core, from center to inner circumference of tube section

σ_{cp} : Compressive strength of plain concrete

σ_c : Cylinder strength of concrete

The elastic modulus and maximum strain of unconfined concrete is suggested that;

$$E_c = (6.9 + 3.32\sqrt{\sigma_{cp}})10^3 \tag{5.4}$$

$$\varepsilon_{co} = 0.94\sqrt[4]{\sigma_{cp}}\,10^{-3} \tag{5.5}$$

where;

E_c : Elastic modulus of unconfined concrete

ε_{co} : Strain at maximum strength of unconfined concrete, σ_c

As axial load applied to CFT column, a tensile hoop stress exists in the steel tube. This transverse pressure in the steel tube, σ_r is;

$$\sigma_r = -\frac{2t\alpha_u\sigma_s}{D-2t} \tag{5.6}$$

where;

σ_r : Hoop stress on the steel tube

D : Diameter of steel tube

t : Thickness of steel tube

α_u : Normalized hoop stress in circular steel tube at ultimate load, (taken as *-0.19*)

σ_s : Strength of steel tube

The hoop stress generates a lateral pressure, which acts on the surface of the concrete core, so in fill concrete is pressurized triaxially. The amount of lateral pressure on the concrete core is;

$$\sigma_{re} = \frac{k}{k_e}\sigma_r \tag{5.7}$$

where;

σ_{re} : Confining stress on the concrete provided by steel section

k : Confinement coefficient, (taken as *4.1*)

k_e : An empirical value, taken as *23*

For the confined concrete maximum peak strength, σ_{ccB} is suggested as;

$$\sigma_{ccB} = \sigma_{cp} + k\sigma_r \tag{5.8}$$

In order to find strain at the maximum confined stress value, "strength enhancement coefficient factor", K, must be calculated. It is;

$$K = 1 - k\left(\frac{2t}{D-2t}\right)\frac{\alpha_u \sigma_s}{\sigma_{cp}} \tag{5.9}$$

Then strain of peak stress of concrete due to confinement effect, ε_{ccB} will be;

$$\varepsilon_{cco} = \begin{cases} \varepsilon_{co} + 4.7\varepsilon_{co}(K-1), & when\ K \le 1.5 \\ 3.4\varepsilon_{co} + 20\varepsilon_{co}(K-1), & when\ K > 1.5 \end{cases} \tag{5.10}$$

The non-dimensional parameters V and M**,** to express stress–strain relation for concrete are proposed as;

$$V = E_c \frac{\varepsilon_{cco}}{\sigma_{ccB}} \tag{5.11}$$

$$W = 1.5 - 17.1 \cdot 10^{-3}\sigma_{cp} + 2.39\sqrt{\sigma_{re}} \tag{5.12}$$

It is seen from this material model that the strength enhancement of concrete due to the confinement effect is involved only with the geometric characteristics and the material strength of steel section. Column shape also has an effect on the lateral pressure. Sakino proposes a modified version of this model for square and rectangular CFT columns. The value of the axial load exerted on the composite column is not taken place in the equation of the lateral pressure provided by the hollow section to concrete; however, it is known that axial load is determinative on the confining pressure on CFT columns [2].

5.2. Steel Model

In order to consider the effect of the biaxial stress state in circular steel tube, it is assumed that the biaxial stresses satisfy the Von Mises yield criterion at the point of yield strength of the CFT members, as shown in Figure 3.1. The compressive yield stress is reduced to 0.91 σ_s and the tensile yield stress was increased to 1.08 σ_s , where σ_s denotes the yield stress obtained from the material coupon tests [1], as mentioned previously. The multipliers 0.91 and 1.08 were determined from the Von Mises yield criterion as;

$$\sigma_s = \sigma_{s\phi}^2 - \sigma_{s\phi}\sigma_{sz} + \sigma_{sz}^2 \tag{5.13}$$

where;

$\boldsymbol{\sigma_s}$: Yield strength of steel

$\boldsymbol{\sigma_{s\theta}}$: Radial stress on the steel tube at the ultimate load

$\boldsymbol{\sigma_{sz}}$: Axial stress on the steel tube at the ultimate load

The components of steel yield stress can be suggested in such a way that;

$$\sigma_{s\phi} = \alpha_u \sigma_s \tag{5.14}$$

$$\sigma_{sz} = \beta_{uc} \sigma_s \tag{5.15}$$

where;

$\boldsymbol{\alpha_u, \beta_{uc}}$: Normalized hoop stress and axial stress in circular steel tube at ultimate load

These components are independent of the steel and concrete strength, the D/t ratio of the steel tube. They are statistically obtained from the compression tests of the CFT stub columns upon reaching ultimate strength.

As represented in Figure 5.1, the stress–strain relationship of a circular tube is assumed bilinear by taking into consideration the strain-hardening effect. There are two different elasticity moduluses, which are based on the results of the coupon tests of the steel tubes. Strength deterioration caused by the local buckling of the steel tube is not taken into account in this test. The mathematical expressions of the stress–strain relationships of the circular tubes are shown in the following equations;

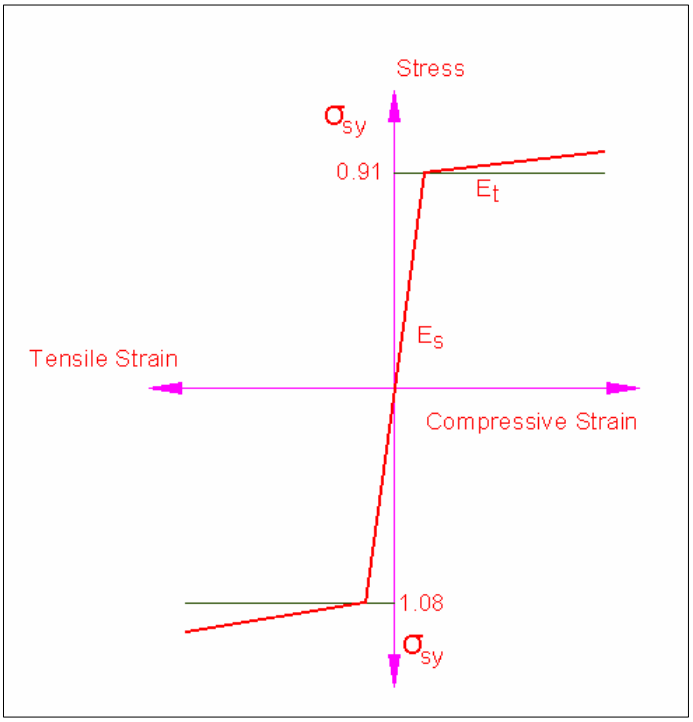

Figure 5.1. Stress-strain figure of steel tube used in FSA.

$$\varepsilon_s = \frac{\sigma_s}{E_s} \tag{5.16}$$

$$\varepsilon_{sc} = 0.91\varepsilon_s \tag{5.17}$$

$$\varepsilon_{st} = 1.08\varepsilon_s \tag{5.18}$$

$$E_t = \frac{\sigma_{st} - \sigma_s}{\varepsilon_{su} - \varepsilon_s} \tag{5.19}$$

where;

$\boldsymbol{\varepsilon_s}$: Strain at yield strength of steel, σ_s

$\boldsymbol{E_s}$: Elastic modulus of steel

$\boldsymbol{E_t}$: Inelastic modulus of steel

$\boldsymbol{\varepsilon_{sc}}$, $\boldsymbol{\varepsilon_{st}}$: Strain at yield strength of steel in the case of compression and tension, respectively

$\boldsymbol{\sigma_{st}}$: Tensile strength of the steel tube

$\boldsymbol{\varepsilon_{su}}$: Strain at tensile strength, σ_{st}

When steel is under compression, the stress on the steel tube is;

$$\sigma = \begin{cases} \varepsilon E_s & ,when\ \varepsilon \le \varepsilon_{sc} \\ 0.91\sigma_s + E_t(\varepsilon - \varepsilon_{sc}) & ,when\ \varepsilon \ge \varepsilon_{sc} \end{cases} \tag{5.20}$$

When steel is under tension, the stress on the steel tube is;

$$\sigma = \begin{cases} \varepsilon E_s & ,when\ \varepsilon \le \varepsilon_{st} \\ 1.08\sigma_s + E_t(\varepsilon - \varepsilon_{st}) & ,when\ \varepsilon \ge \varepsilon_{st} \end{cases} \tag{5.21}$$

6. SAKINO'S EXPERIMENTAL RESEARCH

In this thesis study, the required experimental data was obtained from a research paper written by Fujimoto [1] in order to use for the verification of generated analysis program by using FSA technique. The experimental moment-curvature diagrams of each specimens were discretized point by point from this research text.

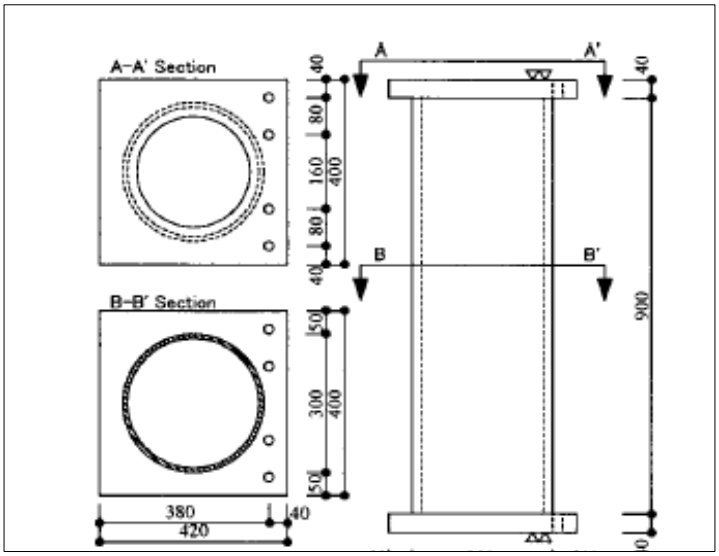

Figure 6.1. The details of specimens

The details of typical specimens presented in Fujimoto's study are shown in Figure 6.1. A total of 18 circular composite specimen had been tested by Fujimoto. The test parameters had been determined as follows,

- nominal tensile strength of steel tubes
- concrete strength
- diameter- to-thickness ratio of steel tubes
- axial force ratio
- applied axial force

It is reported that, the circular tubes are cold-formed from a flat plate by press bending and seam welding. The ratio of the specimen clear height to diameter is 3.0.

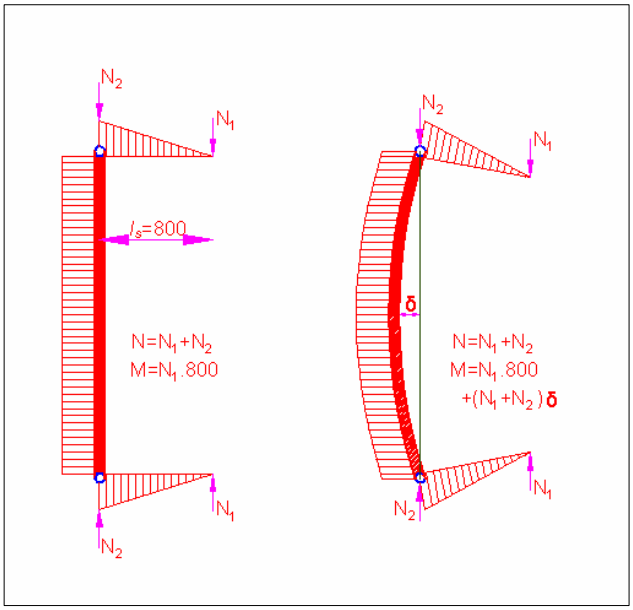

Figure 6.2. Loading schema of specimens

The specimens had been tested under the loading conditions shown in Figure 6.2. Accordingly, constant axial force N (N_2=N, N_1=0) is first applied to the specimen by the testing machine. Then, a monotonously increasing moment is applied to the specimen by increasing axial force N_1. The concentric axial force, N_2, applied by the test equipment is adjusted for each change in the eccentric force N_1 so that total axial force of N $(=N_1+ N_2)$ would remain constant as the moment is increased. As a result of the horizontal deflection of the specimens bent during the tests, the moment at midheight of the specimens is the sum of the moment applied, $N_1.l_e$, and the secondary moment $(N_1+N_2).\delta$.

It is reported in this paper that, the longitudinal displacements, lateral displacements, and curvatures of the specimens were measured by displacement transducers in the experiment of circular CFT columns. The longitudinal and transverse strain on the outer surfaces of the steel tubes was measured by strain gauges.

The geometrical, material properties and the axial load on the circular CFT columns were also taken from this paper and presented in Table 6.1. These inputs of specimens were entered to the developed FSA program and these specimens were analyzed by computer.

Table 6.1. The geometrical and material properties of specimens

	Specimen	D *(mm)*	t *(mm)*	σ_s *(Mpa)*	σ_c *(Mpa)*	σ_{st} *(Mpa)*	E_s *(Gpa)*	ε_{su} *(%)*	N *(kN)*	N/N_o
1	***EC4-A-4-035***	150	2,96	283	39,9	408	224	29,1	359	0,35
2	***EC4-A-4-06***	150	2,96	283	39,9	408	224	29,1	616	0,59
3	***EC4-C-8-045***	300	2,96	283	77,6	408	224	29,1	2720	0,45
4	***EC4-C-8-06***	300	2,96	283	77,6	408	224	29,1	3627	0,60
5	***EC4-D-4-04***	450	2,96	283	39,9	408	224	29,1	2968	0,40
6	***EC4-D-4-06***	450	2,96	283	39,9	408	224	29,1	4452	0,60
7	***EC6-A-4-02***	122	4,54	579	39,9	646	228	15,2	273	0,20
8	***EC6-A-4-06***	122	4,54	579	39,9	646	228	15,2	817	0,60
9	***EC6-C-8-03***	239	4,54	579	77,6	646	228	15,2	1556	0,30
10	***EC6-C-8-06***	239	4,54	579	77,6	646	228	15,2	3113	0,60
11	***EC6-D-4-03***	360	4,54	579	39,9	646	228	15,2	2050	0,30
12	***EC6-D-4-06***	360	4,54	579	39,9	646	228	15,2	4099	0,60
13	***EC8-A-4-015***	108	6,47	835	39,9	879	218	10,1	300	0,15
14	***EC8-A-4-06***	108	6,47	835	39,9	879	218	10,1	1200	0,60
15	***EC8-C-8-06***	222	6,47	835	77,6	879	218	10,1	3789	0,60
16	***EC8-C-8-07***	222	6,47	835	77,6	879	218	10,1	4421	0,70
17	***EC8-D-4-015***	336	6,47	835	39,9	879	218	10,1	1331	0,15
18	***EC8-D-4-045***	336	6,47	835	39,9	879	218	10,1	3984	0,45

7. ANALYSIS RESULTS AND DISCUSSION

The FSA analysis program developed for the analysis of circular CFT columns were tested by using the experiment results of Fujimoto, as mentioned earlier. The moment–thrust curvature relationships of the CFT columns were also numerically derived using the fiber analysis method by Fujimoto. The experimental and analysis results of 18 circular CFT columns with FSA results are presented and compared in the "Moment-Curvature Graphs" from Figure 7.1 to Figure 7.18. The peak moments obtained from experimental, numerical and FSA study is tabulated in Table 7.1.

Table 7.1. Peak moment values of specimens found by experiment, numeric study and FSA.

	M_{exp} (kN.m)	M_{num} (kN.m)	M_{FSA} (kN.m)	$\Delta_{exp-FSA}$ (%)	$\Delta_{exp-num}$ (%)	$\Delta_{num-FSA}$ (%)
EC4-A-4-035	31.65	29.26	29.20	*7.8*	*7.6*	*0.2*
EC4-A-4-06	26.23	24.61	25.17	*4.0*	*6.2*	*-2.3*
EC4-C-8-045	194.08	216.11	211.85	*-9.2*	*-11.4*	*2.0*
EC4-C-8-06	154.11	170.77	173.68	*-12.7*	*-10.8*	*-1.7*
EC4-D-4-04	406.80	423.75	412.48	*-1.4*	*-4.2*	*2.7*
EC4-D-4-06	339.00	313.58	318.99	*5.9*	*7.5*	*-1.7*
EC6-A-4-02	45.77	45.77	45.31	*1.0*	*0.0*	*1.0*
EC6-A-4-06	41.53	37.29	38.69	*6.8*	*10.2*	*-3.8*
EC6-C-8-03	216.11	228.83	227.4	*-5.2*	*-5.9*	*0.6*
EC6-C-8-06	177.98	173.74	185.29	*-4.1*	*2.4*	*-6.6*
EC6-D-4-03	457.63	488.14	486.07	*-6.2*	*-6.7*	*0.4*
EC6-D-4-06	396.61	366.10	388.03	*2.2*	*7.7*	*-6.0*
EC8-A-4-015	48.01	64.54	63.94	*-33.2*	*-34.4*	*0.9*
EC8-A-4-06	52.81	48.01	51.65	*2.2*	*9.1*	*-7.6*
EC8-C-8-06	260.20	255.10	279.72	*-7.5*	*2.0*	*-9.7*
EC8-C-8-07	257.14	209.18	246.05	*4.3*	*18.7*	*-17.6*
EC8-D-4-015	596.62	759.33	747.27	*-25.3*	*-27.3*	*1.6*
EC8-D-4-045	661.70	683.40	706.1	*-6.7*	*-3.3*	*-3.3*

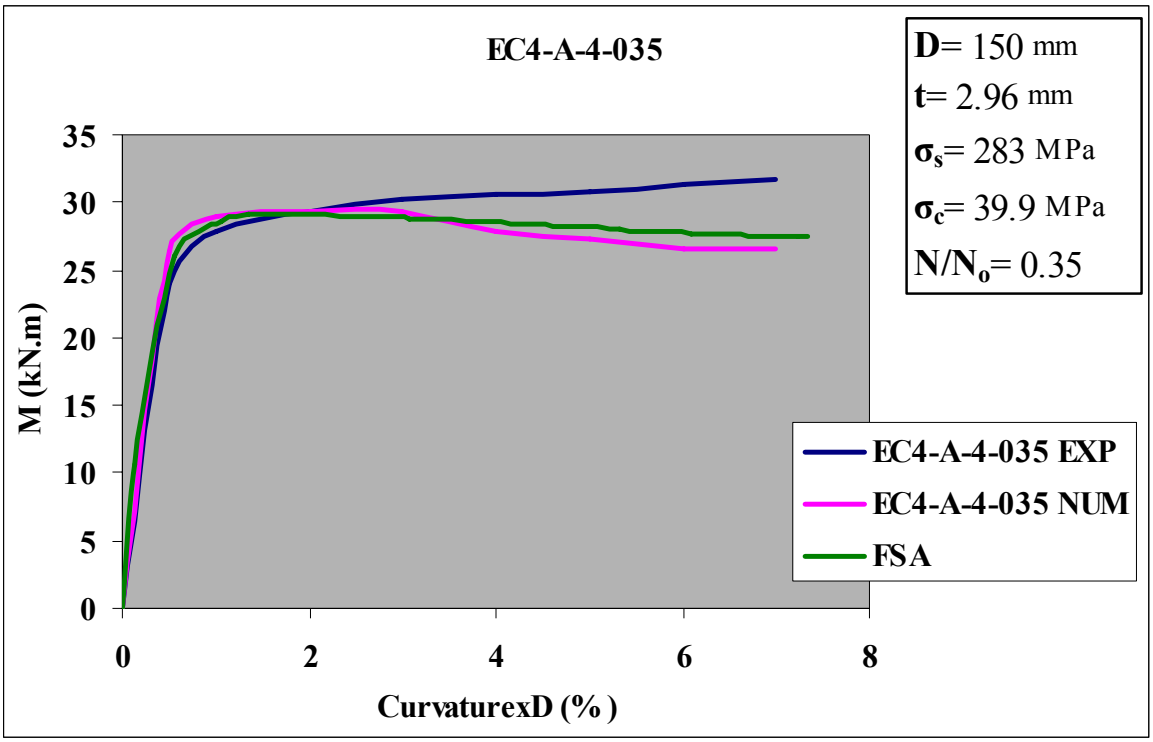

Figure 7.1. M vs. φ diagrams of specimen EC4-A-4-035

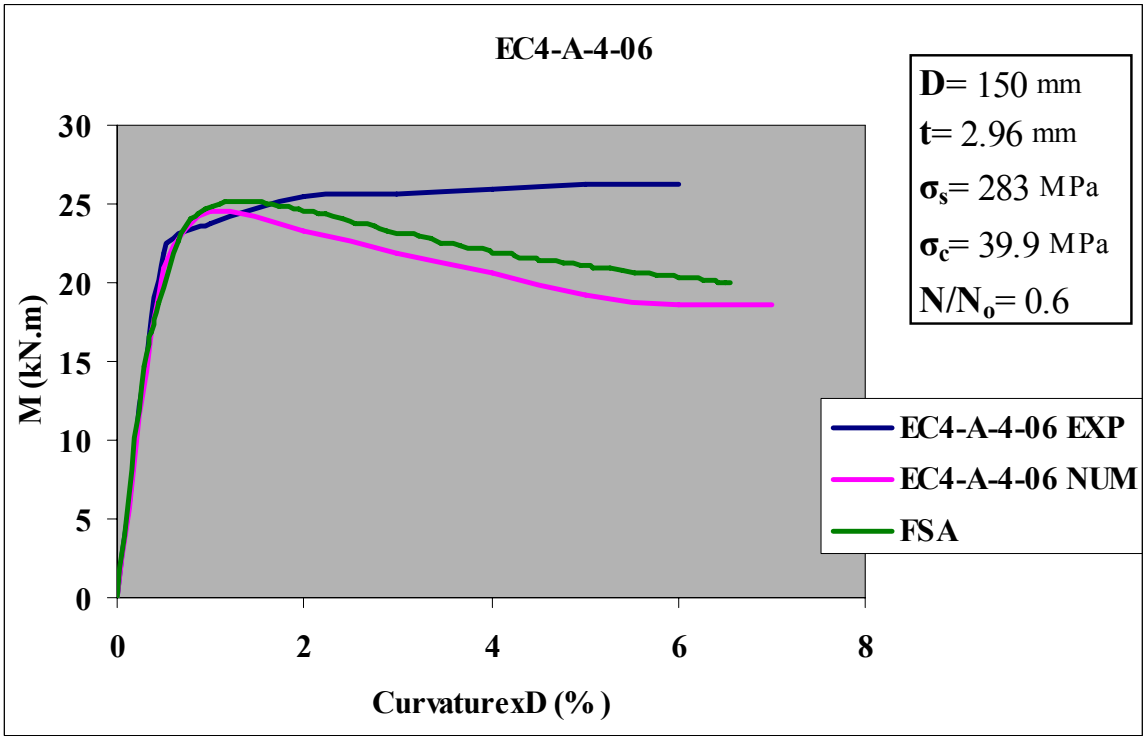

Figure 7.2. M vs. φ diagrams of specimen EC4-A-4-06

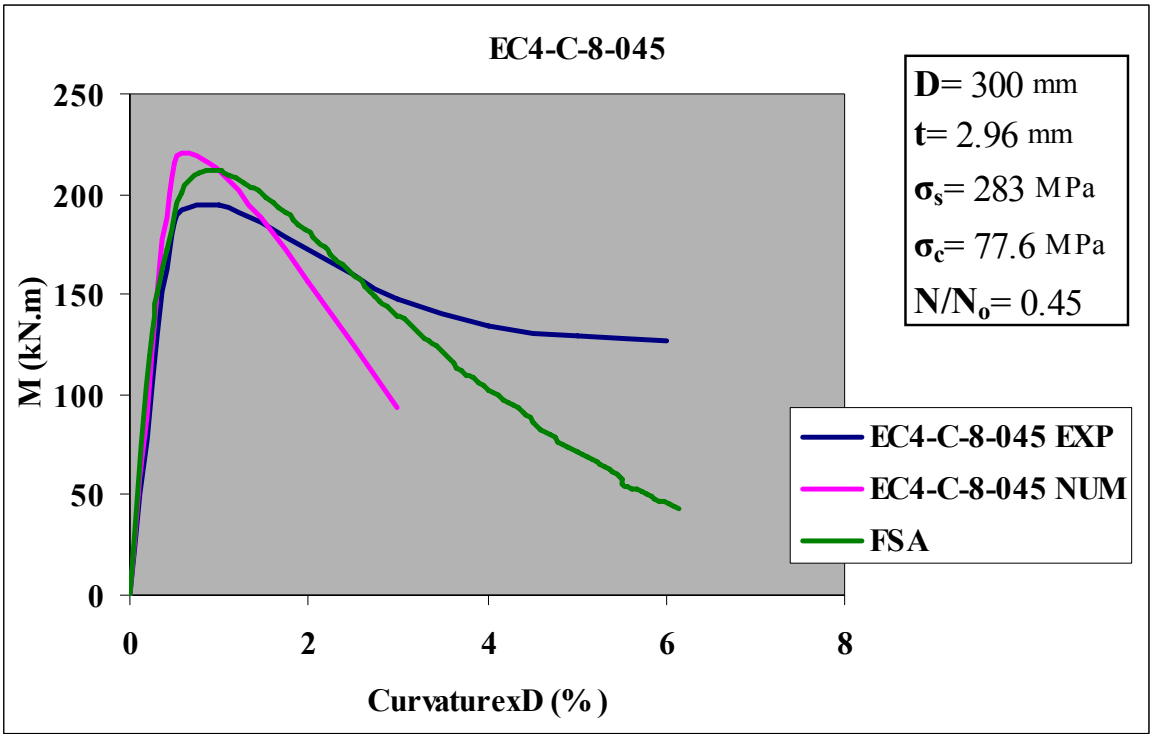

Figure 7.3. M vs. φ diagrams of specimen EC4-C-8-045

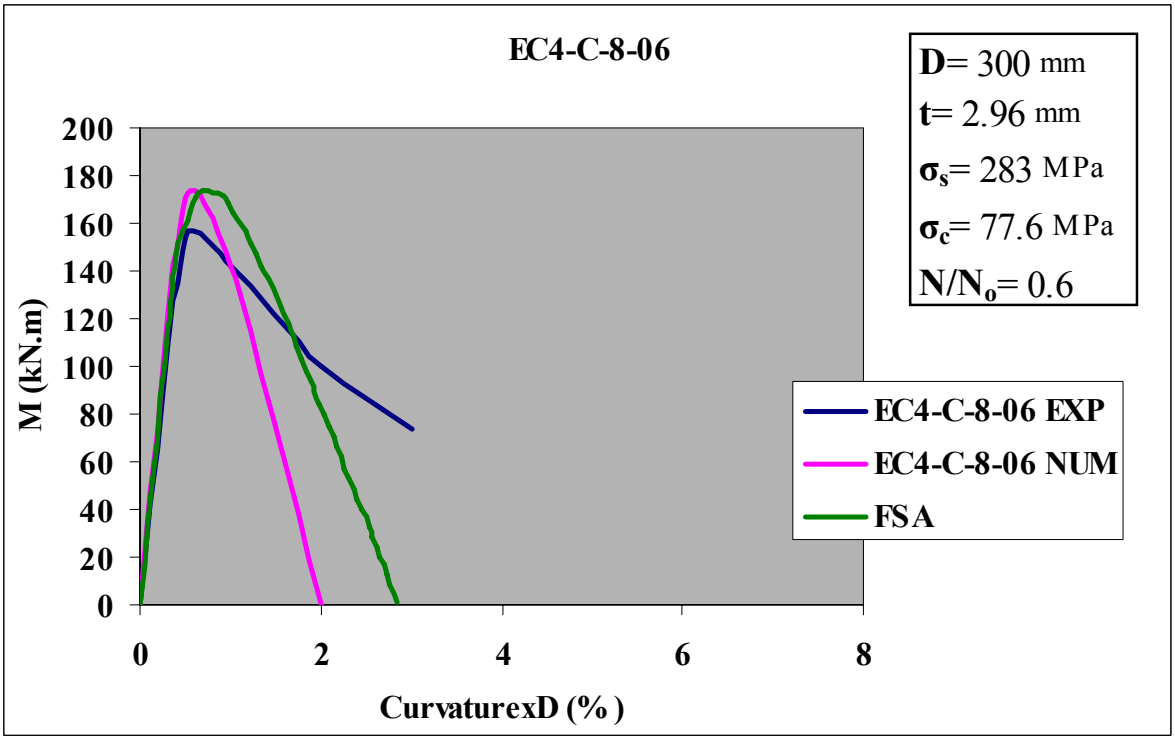

Figure 7.4. M vs. φ diagrams of specimen EC4-C-8-06

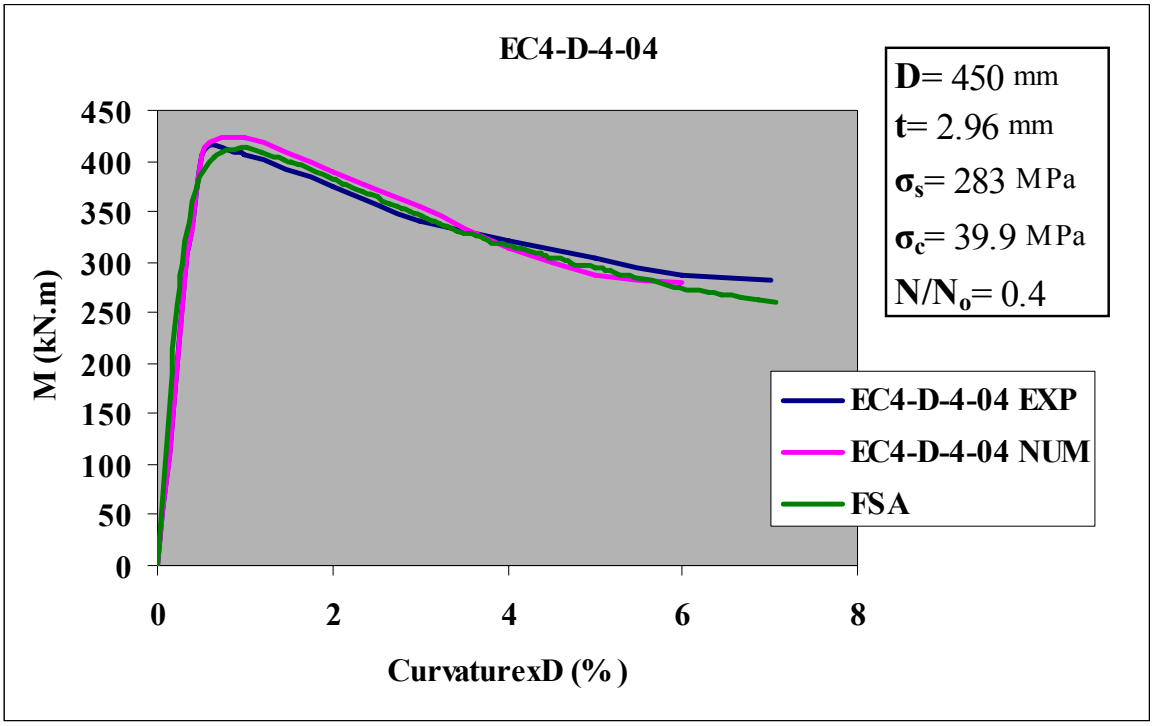

Figure 7.5. M vs. φ diagrams of specimen EC4-D-4-04

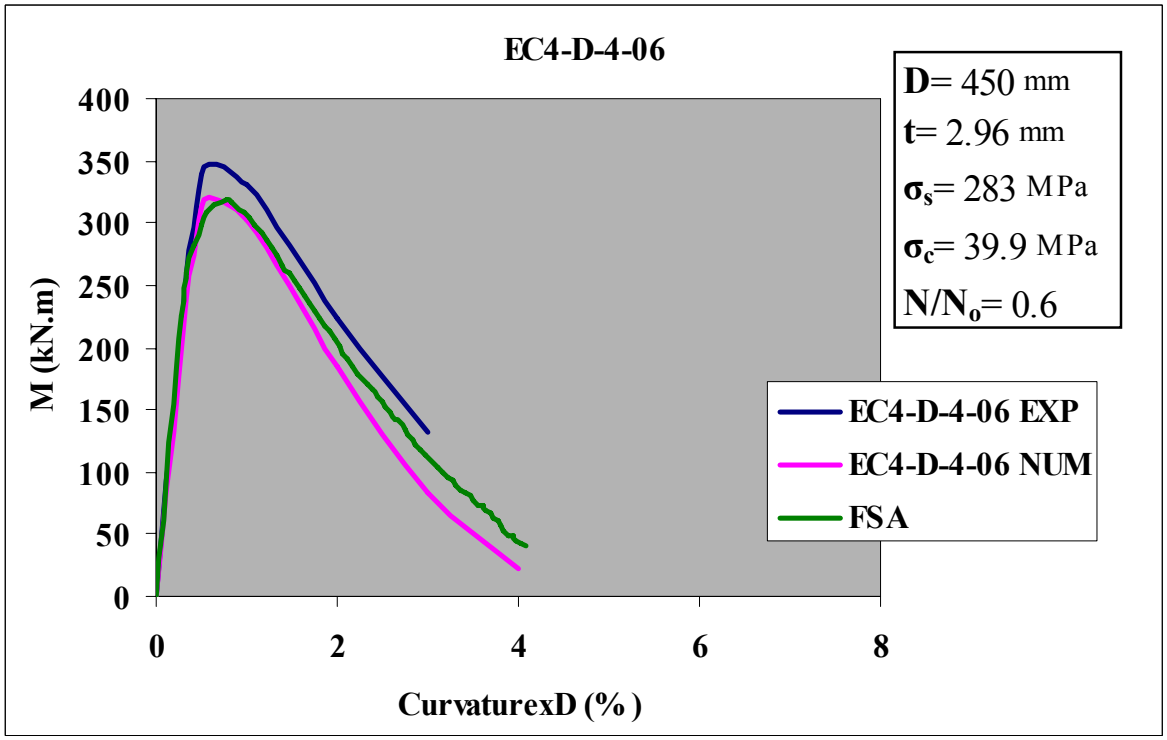

Figure 7.6. M vs. φ diagrams of specimen EC4-D-4-06

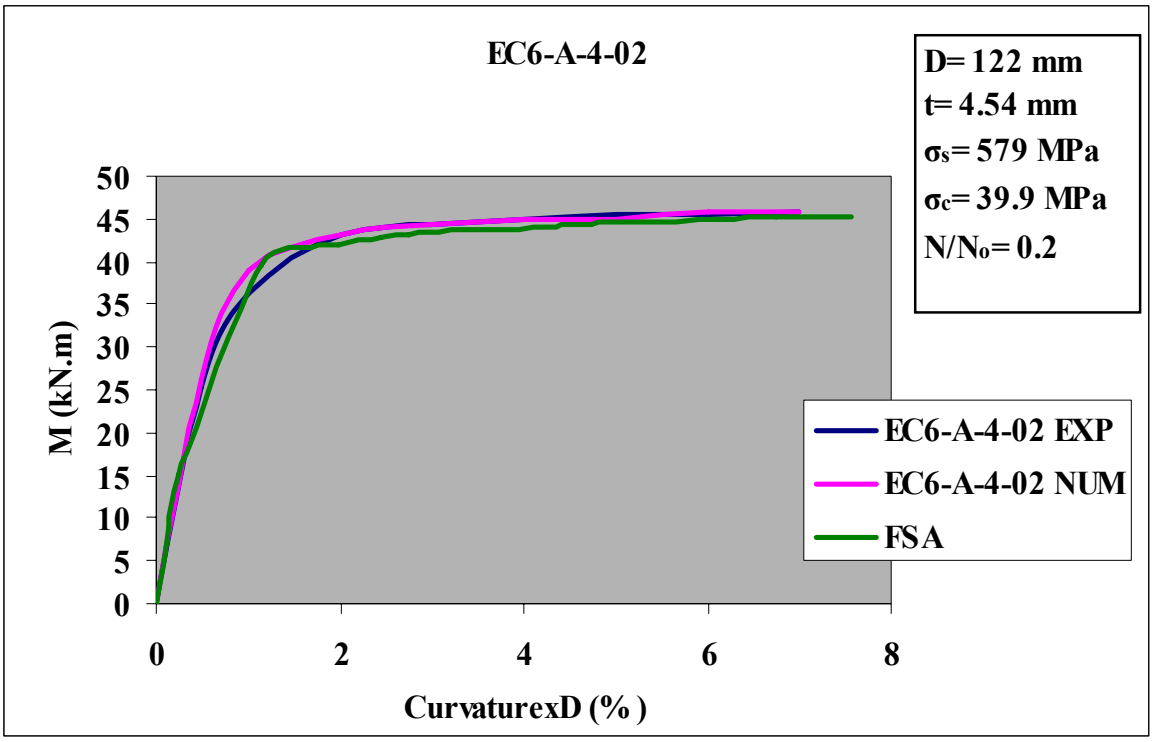

Figure 7.7. M vs. φ diagrams of specimen EC6-A-4-02

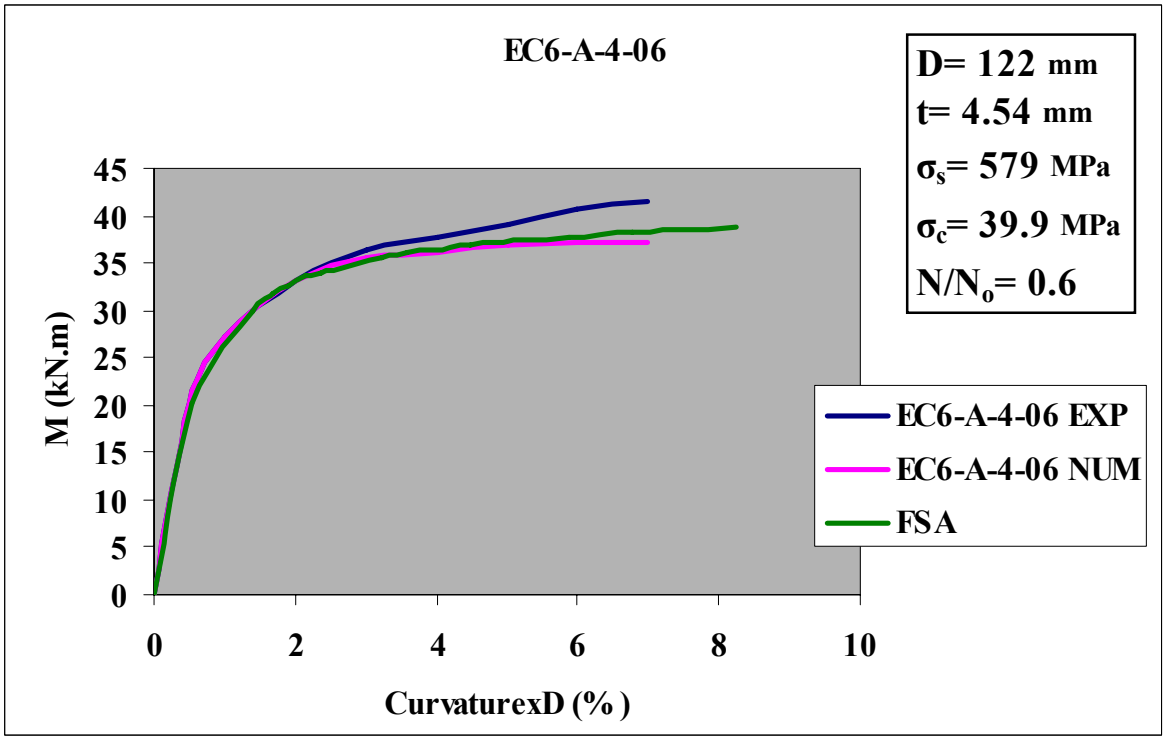

Figure 7.8. M vs. φ diagrams of specimen EC6-A-4-06

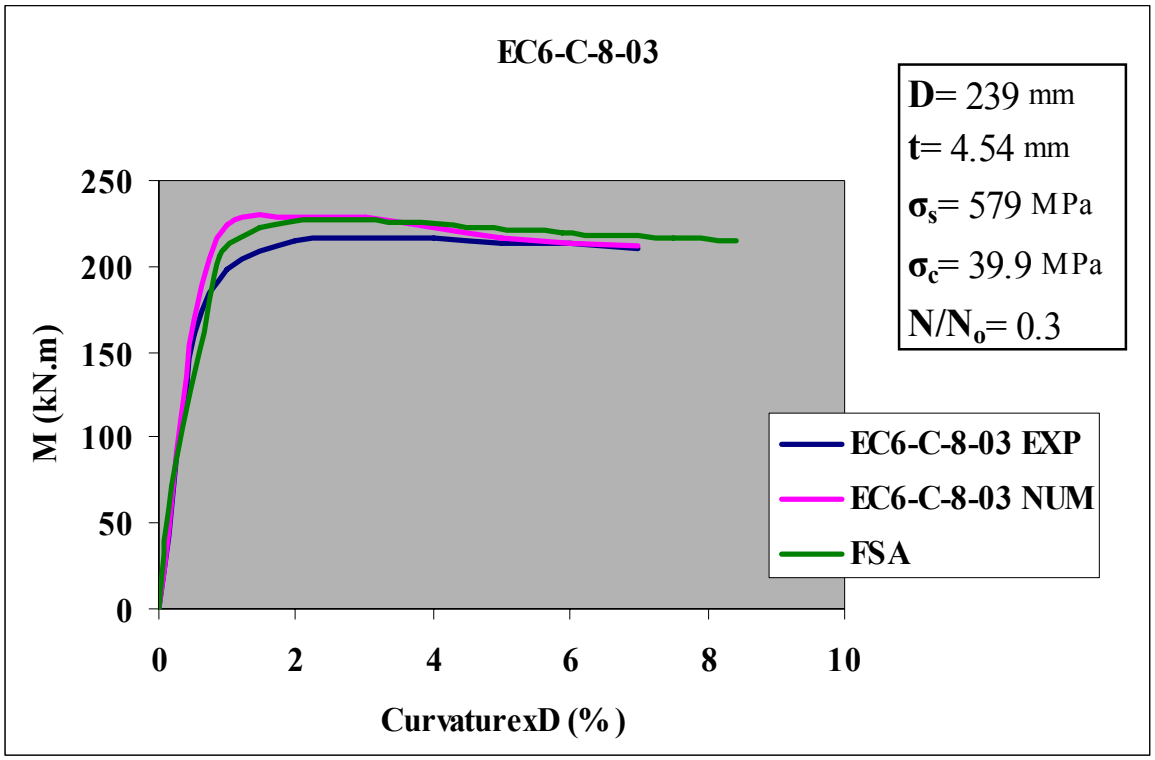

Figure 7.9. M vs. φ diagrams of specimen EC6-C-8-03

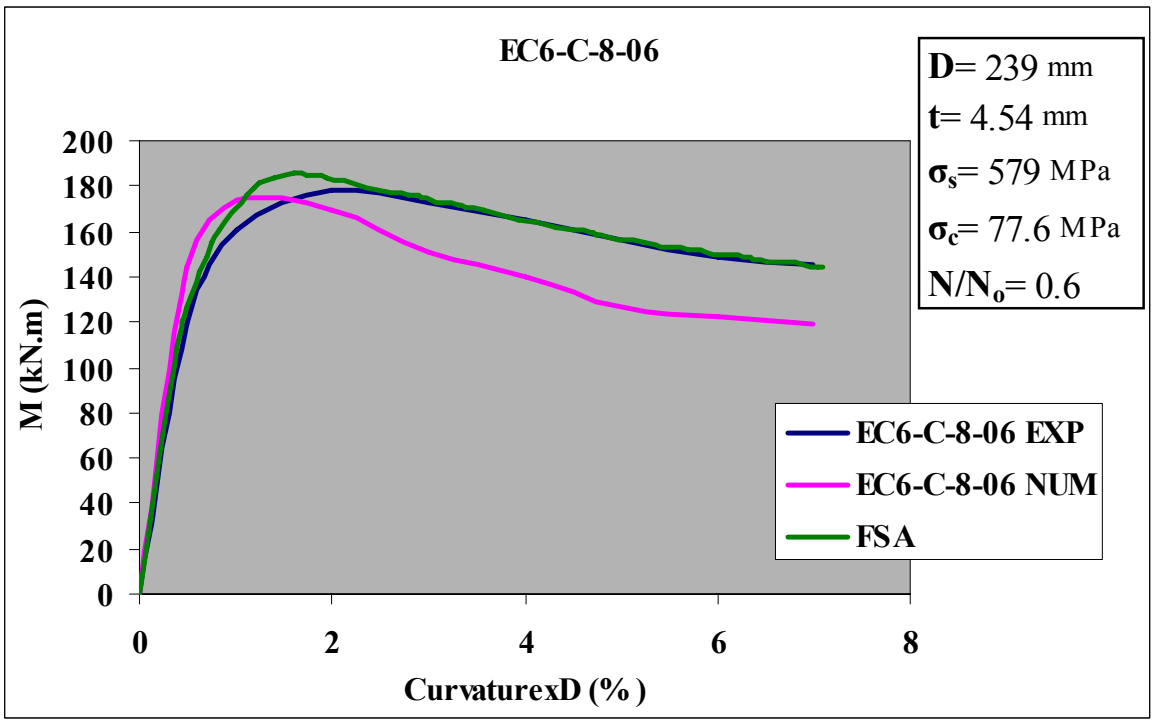

Figure 7.10. M vs. φ diagrams of specimen EC6-C-8-06

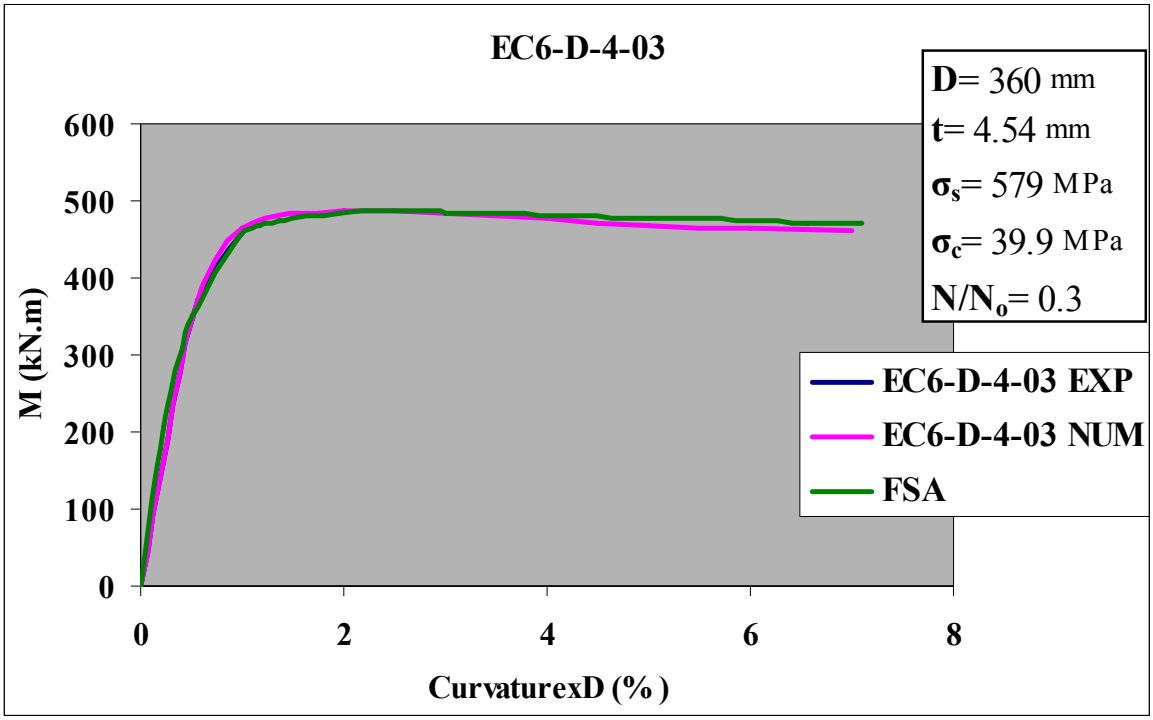

Figure 7.11. M vs. φ diagrams of specimen EC6-D-4-03

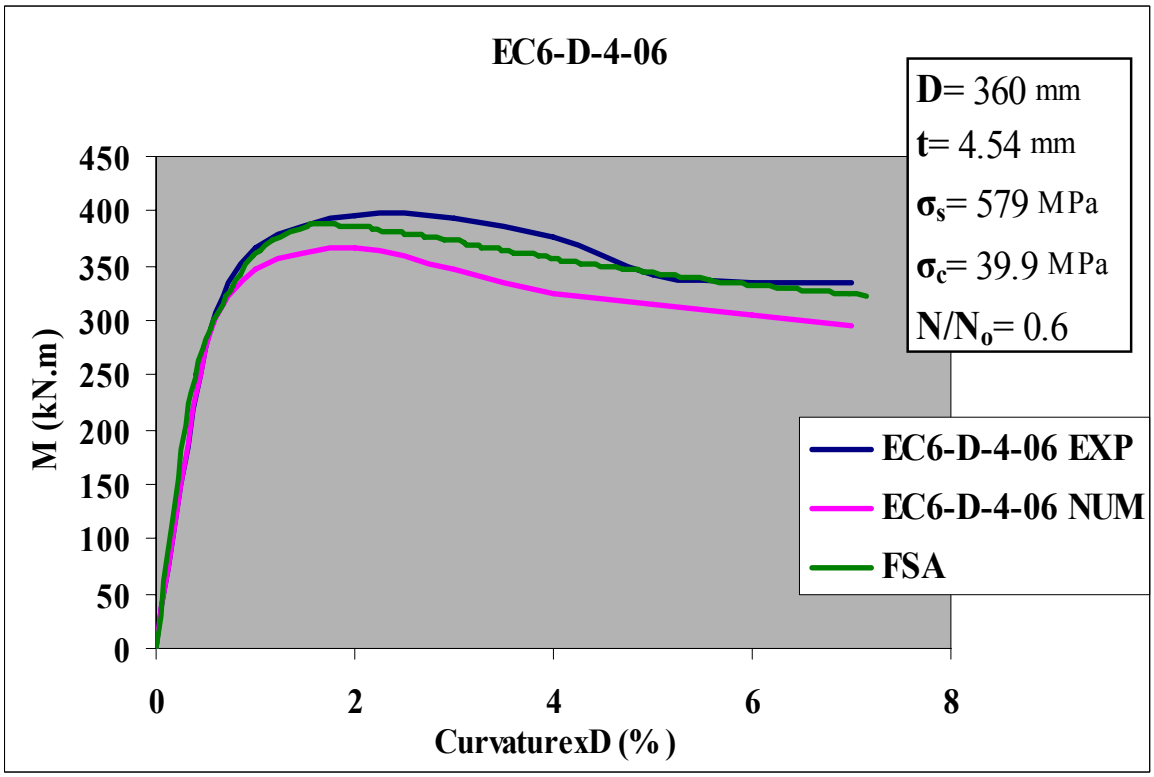

Figure 7.12. M vs. φ diagrams of specimen EC6-D-6-06

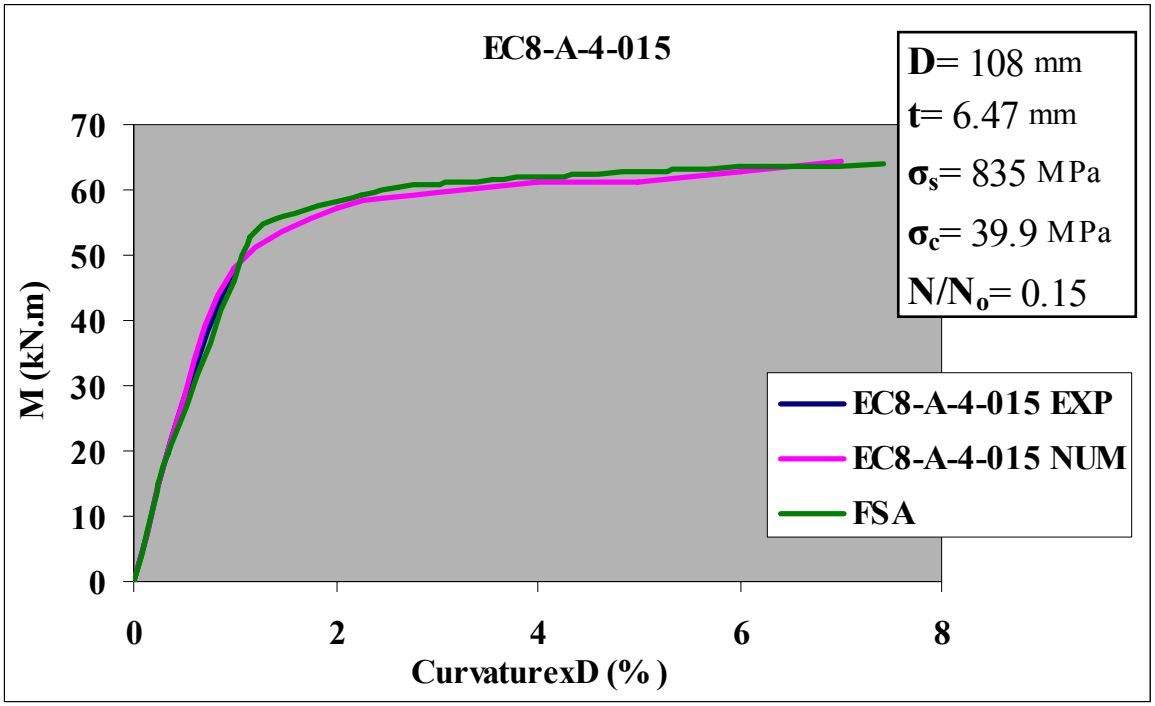

Figure 7.13. M vs. φ diagrams of specimen EC8-A-4-015

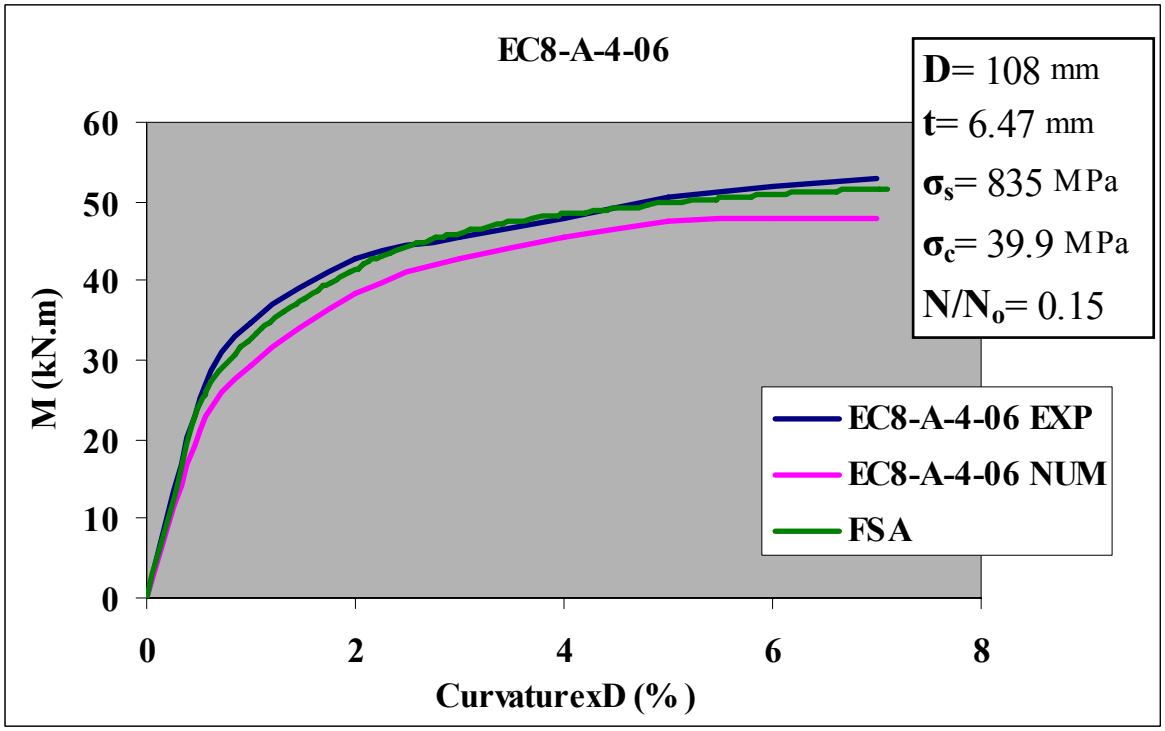

Figure 7.14. M vs. φ diagrams of specimen EC8-A-4-06

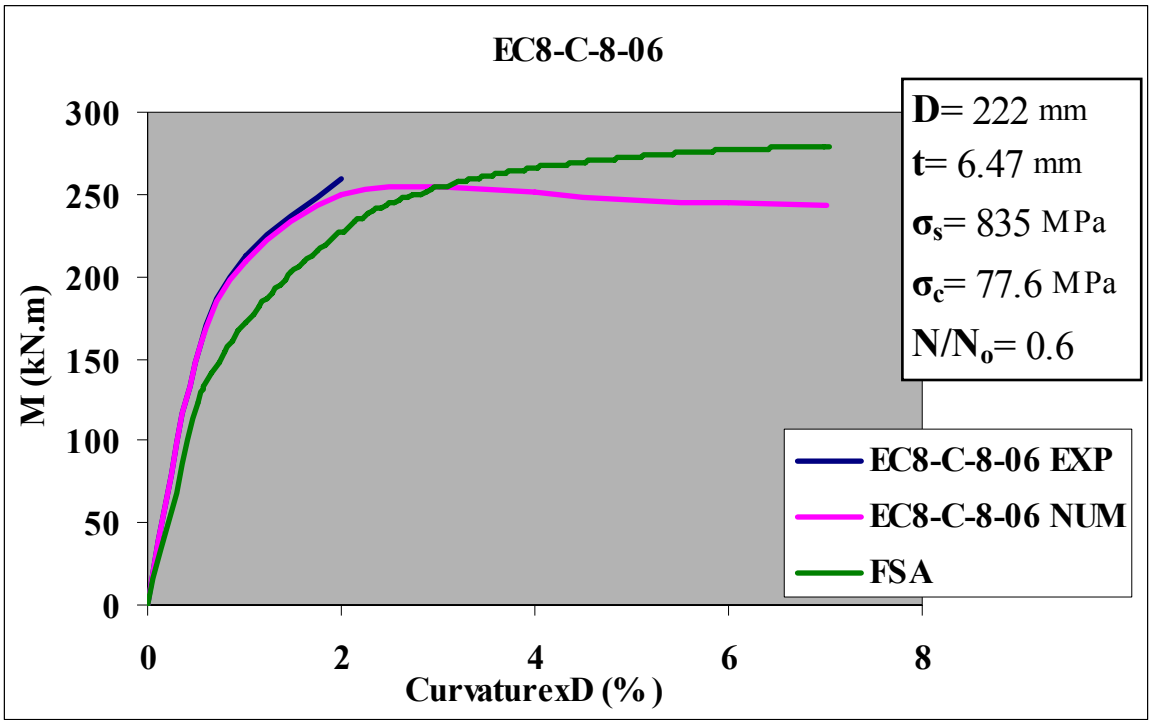

Figure 7.15. M vs. φ diagrams of specimen EC8-C-8-06

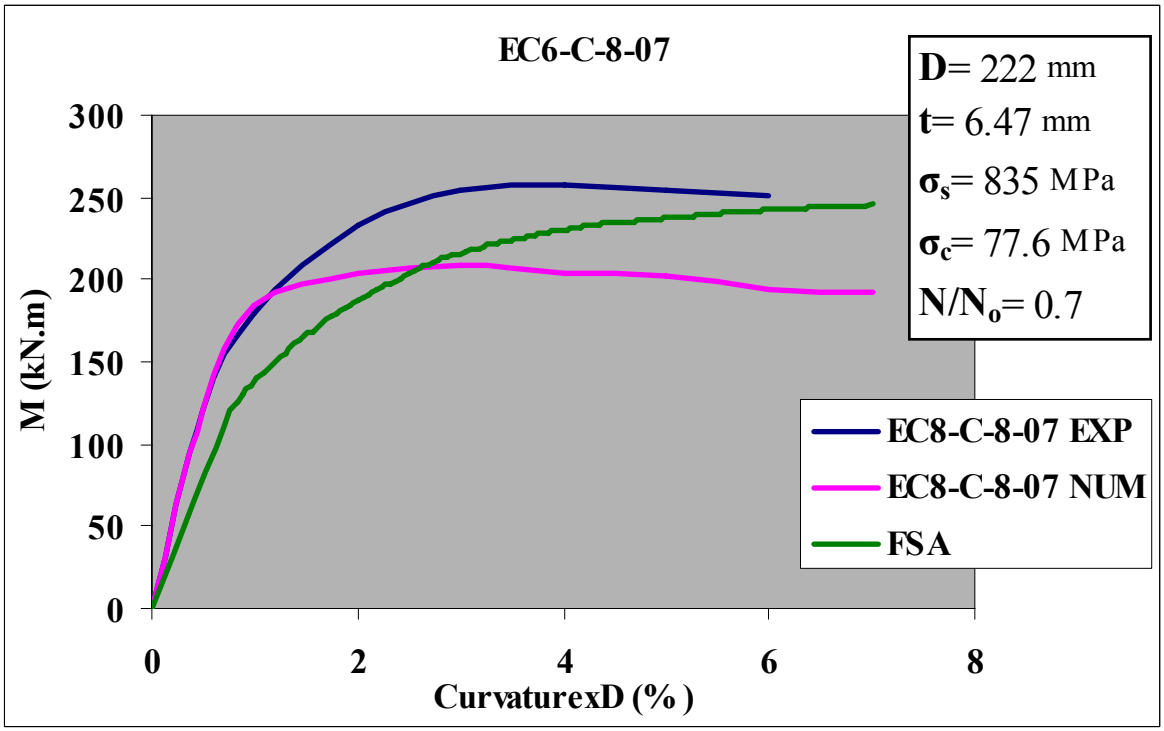

Figure 7.16. M vs. φ diagrams of specimen EC8-C-8-07

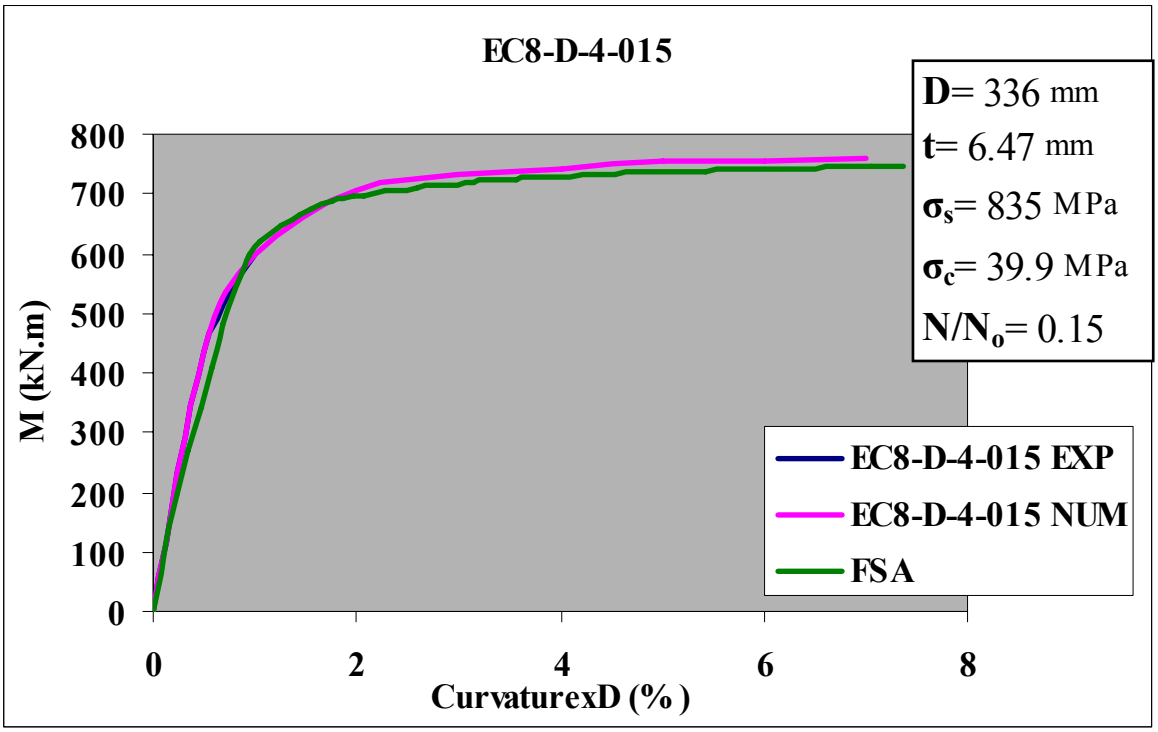

Figure 7.17. M vs. φ diagrams of specimen EC8-D-4-015

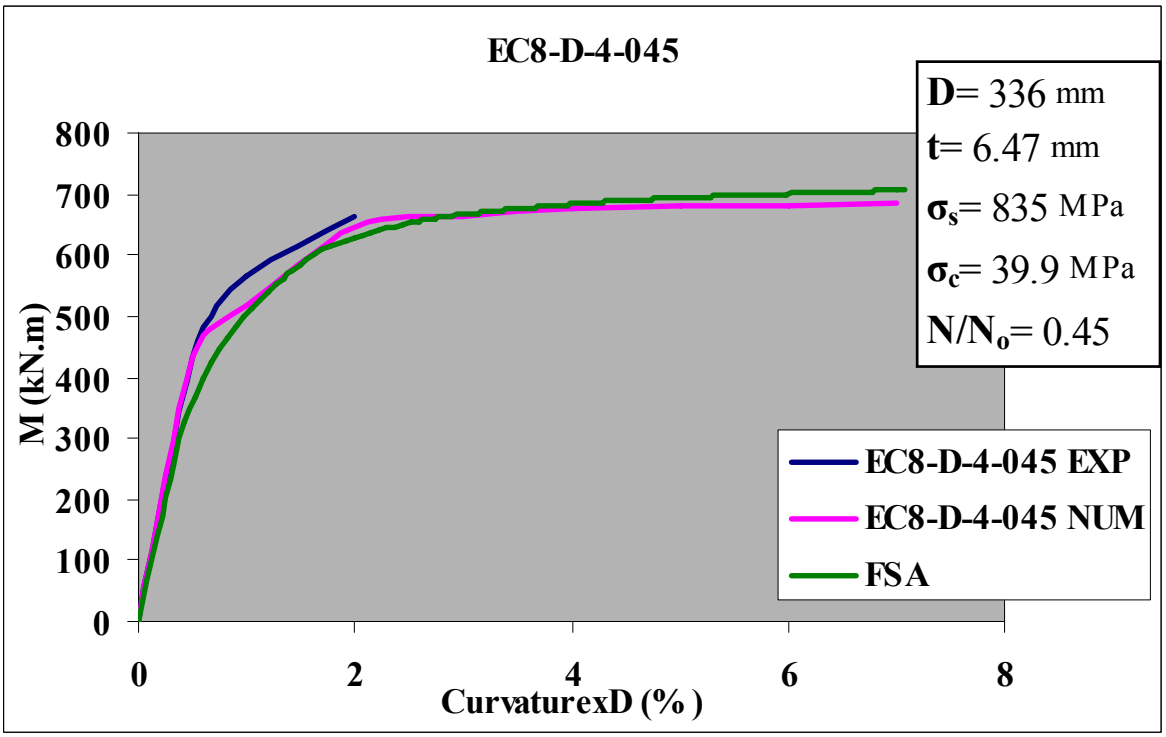

Figure 7.18. M vs. φ diagrams of specimen EC8-D-4-045

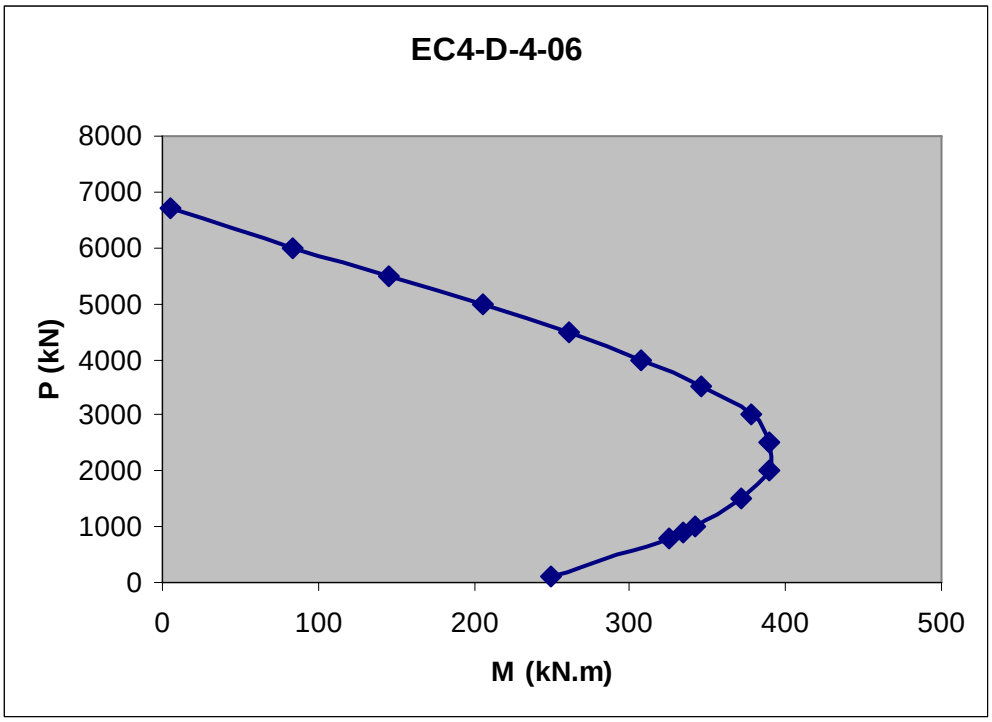

Figure 7.19. P-M interaction diagram of specimen EC4-D-4-06

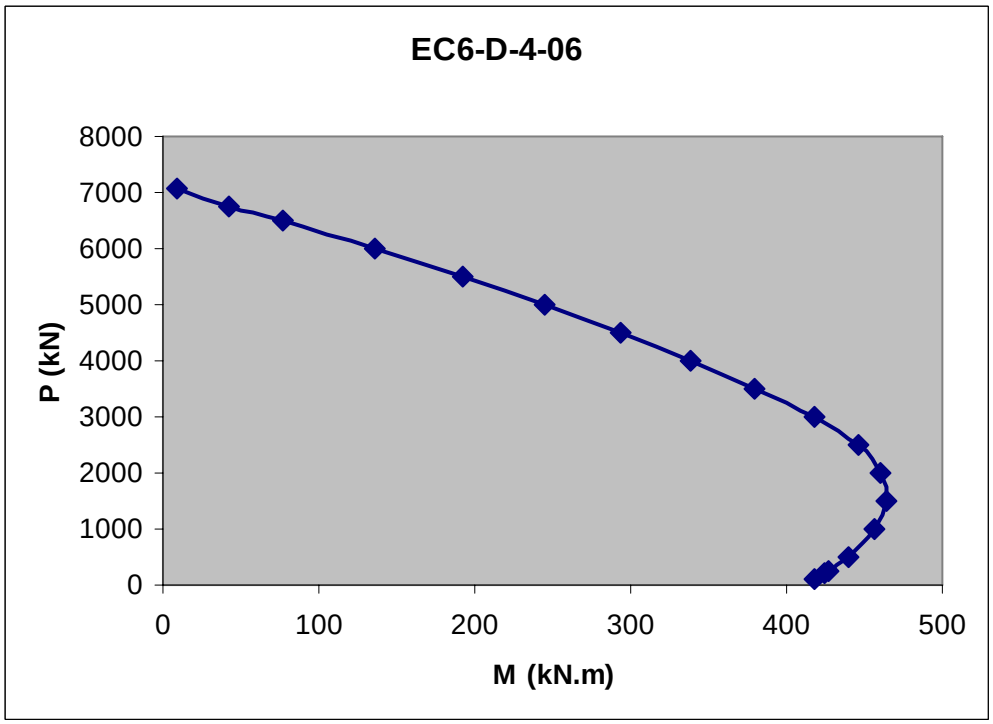

Figure 7.20. P-M interaction diagram of specimen EC6-D-4-06

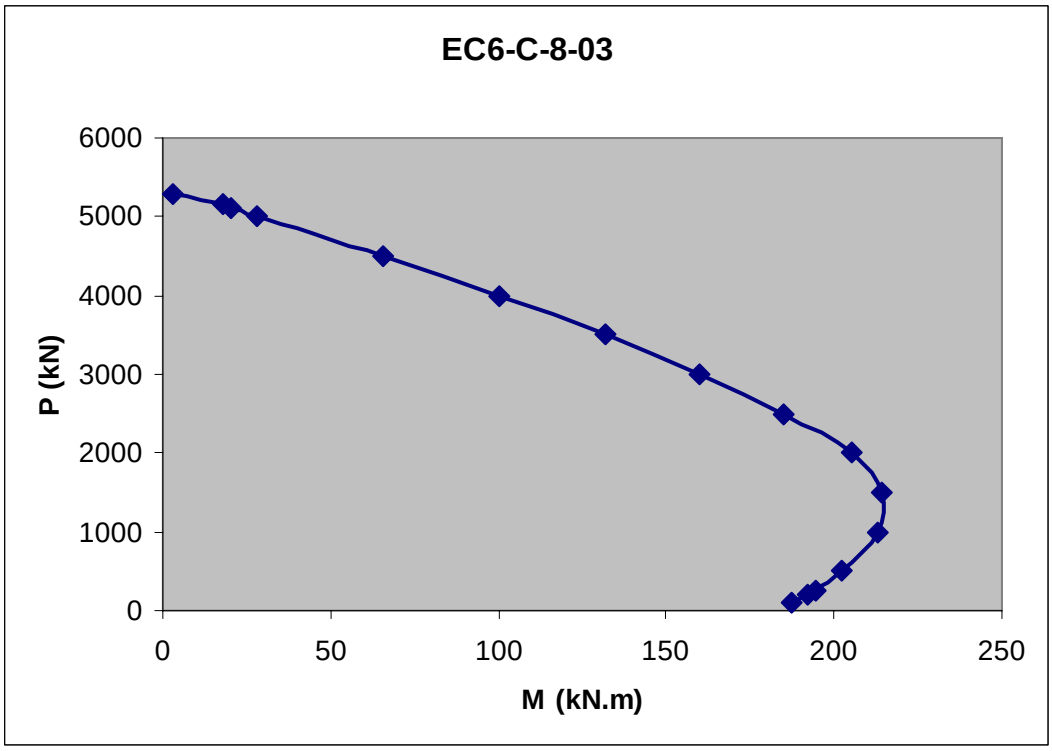

Figure 7.21. P-M interaction diagram of specimen EC6-C-8-03

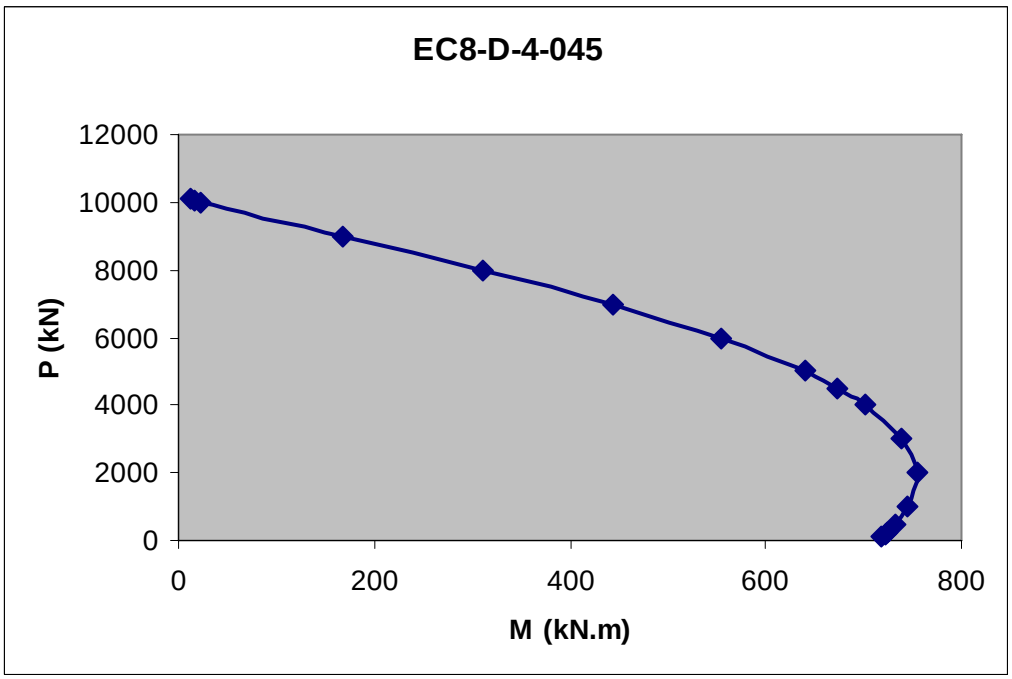

Figure 7.22. P-M interaction diagram of specimen EC8-D-4-045

7.1. Experimental Results vs. FSA Results

The moment vs. curvature graphs of CFT specimens show that, there is a good agreement between the experimental, numerical and FSA results. The peak moments and the ductility of all circular CFT columns are predicted with a high accuracy level. Comparing to the numerical results of the Fujimoto, the FSA results agree with the experimental results better. On the other hand, some differences are also observed for the results of some specimens. These errors can stem from both experimental study and numerical study. In the case of the experimental work; measurements during the tests, poor workmanship of specimens, unexpected steel and concrete material behavior, second order effects, residual stresses on the steel tube etc. may cause these errors. For the analytic study; assumptions for the FSA, using some statistical values i.e. α_u, β_{uc}, numerical integration technique, fiber discretization differences between numerical analysis and FSA, error margin for equilibrium equation, strain and N.A. location increments could lead the divergence of the FSA results form the test results. Apart from the experimental and the numerical study, a possible error may arise from the graphical discretization of test and numerical moment-curvature graphics of Fujimoto's research paper. Even if, it is clarified that the FSA analysis is very rapid and it shows a good performance to predict the circular CFT steel columns behavior.

As stated, the test results of some columns do not agree with the FSA results. For instance, in *EC4-A-4* series columns, it is seen that both FSA and numeric results underestimate the post peak behavior, however experimental results give that specimens can carry greater moment than analysis results. This may stem from low D/t ratio steel tube, which cannot provide adequate confinement to the column.

In *EC4-C-8-045* and *EC4-C-8-06,* the behaviors of these columns are predicted to be more brittle by FSA but the experiments show that their behaviors are ductile in reality. Similarly, in *EC8-C-8-06* and *EC8-C-8-07* tubes, the behavior is more ductile with respect to the experiments, however it is anticipated from the FSA that tubes are brittle. It can be concluded that steel tubes implement greater lateral pressure to concrete core although D/t ratio and axial load of the columns are high.

By comparing *EC4*, *EC6* and *EC8* columns, it is seen that the slope of the $M - \varphi$ diagram line is directly correlated with the steel tube strength. It is observed that this slope decreases, as the yield strength of steel tube increases, in the elastic region. In the elasto-plastic region, the line of $M - \varphi$ diagram stretches with a smooth and rounded scheme when the steel tube strength increases, as seen in *EC8* column diagrams. Yet, the transition from the elastic to the plastic material behavior is sharp in *EC4* type columns. This situation could be interpreted that there would be an immediate change in the moment on the CFT section while steel tube starts yielding. In plastic region, the line climbs up similarly, however it falls down when steel strength goes down for all three curves.

As summarized in Table 7.1, in *EC4* columns the difference between FSA and experimental peak moments are not great. Only, *EC4-C-8-045* and *EC4-C-8-06* columns have great deviations. Since the FSA and the numeric results are close to each other, the reason for this error must be due to the mathematical formulation of material model. In the case of *EC6* series columns, FSA results and experimental results are in a correlation. As seen from the Table 7.1., the peak moments founded by FSA are very close the experimental results. In *EC8* series columns, the peak moments of three columns are greatly different from FSA result. The reason of this situation is the welding cracks between steel tube and end plate occurred during the experiments. Therefore, these columns failed before reaching their peak moment capacities.

7.2. Effect of D/t Ratio

The effect of D/t ratio of steel tube to the moment carrying capacity and ductility can be interpreted by looking their moment vs. curvature graphs. The specimens are marked with *A, C* and *D* letters according to their D/t ratios based on the AIJ building code [1]. *A* is the lowest D/t ratio class and *D* is the highest class. To start with, in *EC4-A-4-035*, *EC4-D-4-040* and *EC4-A-4-06, EC4-D-4-06* columns, as the D/t ratio increases, or concrete fill area increases, the moment carrying capacity of specimens in the plastic region goes down, so ductility decreases. Similar results can be reached by comparing *EC8-A-4-015, EC8-D-4-015* columns. Nevertheless, the ductility slightly changes or not in these

columns. The reason for this fact may be the use of high strength steel tube in composite columns.

In the case of *EC4-C-8-045* and *EC4-C-8-06*, the graphs indicate that specimens are weak at energy absorption capacity. There are two main reasons for this case: high concrete strength and high D/t ratio. Therefore, these columns cannot maintain the peak moment values after the yielding of steel. The behavior of columns deteriorates in terms of ductility. Furthermore, the predicted peak moments are overestimated by FSA. The difference between FSA and test results is directly correlated with the increase of axial load on the specimens. As a result, it can be asserted that FSA using Sakino's concrete model, estimates the behavior of specimens as more brittle in the majority of *EC4* series columns.

7.3. Effect of Steel Strength

The moment vs. curvature diagrams show that steel strength is one of the most significant parameters in the member ductility. When *EC4-A-4-06, EC6-A-4-06* and *EC8-A-4-06; EC4-C-8-06, EC6-C-8-06* and *EC8-C-8-06; EC4-D-4-06* and *EC6-D-4-06* are compared, it is clearly understood that an increase of steel tube strength leads to more ductile behavior in CFT columns.

In *EC8* columns which are built up by high strength steel tubes, whatever the D/t ratio and the concrete strength, after the occurrence of the plastic hinges, the columns exhibit very ductile behavior and high moment enhancement, as shown in the graphs of *EC8-A-4-015* and *EC8-D-4-015*. This situation shows that the steel strength is the most significant factor in the ductility of CFT columns. By comparing *EC8-C-8-06* and *EC8-C-8-07* specimens, although the concrete strength -*80 MPa*- and the axial load are high, adequate ductility can be achieved, by using high strength steel tube.

7.4. Effect of Concrete Strength

The moment vs. curvature graphs also provide information for the concrete strength and the ductility relationship. The test results of specimens are only limited to two different concrete grade; *40* and *80* MPa, respectively. Therefore, direct comments are not possible to make on the effect of concrete strength on CFT ductility. Nevertheless, high concrete strength prescribes CFT column to behave in a brittle manner. *EC4-C* specimens with 80 MPa concrete show the worst performance inside all other specimens in terms of ductility because of the high D/t ratio and concrete strength. Conversely, *EC6-C-8-03* and *EC6-C-8-06* columns perform better than *EC4* columns, due to 600 MPa yield strength of tube. *EC8-C-8-06* and *EC8-C-8-07* columns are very ductile although concrete strength and D/t ratio are great so, the steel tube strength overwhelms the negative effects of D/t ratio and axial load on the member ductility.

7.5. Effect of Axial Load

After drawing moment vs. curvature graphs of specimens, diagrams show that the ductility falls down by the increase of axial load. Indeed, this fact is also valid for the steel beam-columns and the reinforced concrete columns. In order to investigate effect of axial load on the ductility, specimens *EC4-A-4-06* and *EC4-A-4-035; EC4-D-4-06* and *EC4-D-4-04* can be compared. As it is clear, the increase of axial load exerted on the specimens decreases the ductility of columns. On the other hand, *EC6-A-4-06* and *EC6-A-4-02; EC6-D-4-06* and *EC6-D-4-03* specimens exhibit less deterioration in the plastic region. In all *EC8* series columns have the best performance compared to *EC4* and *EC6* specimens. To sum up, the increase of steel strength is a reason for axial load to be less effective on the ductility.

8. CONCLUSION

In this thesis study, the "Fiber Stress Analysis" was performed for circular CFT steel columns. In order to analyze columns, a computer program was developed which includes the mathematical material models of Sakino for steel and concrete. The moment vs. curvature diagrams of specimens tested by Fujimoto were presented for comparison with the test results and FSA results of researcher. It is seen that FSA results have a good agreement with the researcher's test and FSA results. At the end of this study, the following conclusions can be set forth:

1. It is observed that FSA technique, which is a fast and uncomplicated analysis method rather than complex, and time-consuming "Finite Element Analysis" technique, provides quite satisfactory results in the analysis of circular CFT composite columns.

2. As it is anticipated, the assumptions of FSA such as, perfect bonding, strain hardening of steel, planar section on flexure are acceptable for the CFT specimens investigated in this study.

3. Steel tube strength is very effective on the determination of the CFT column behavior. It is verified that as steel strength of tube increases, the ductility of circular CFT columns improves.

4. Diameter to thickness (D/t) ratio has a significant role on ductility. By the time this ratio is great which means the volumetric ratio of concrete is large, the confinement provided by the steel tube is not sufficient to resist moment in high deformation stages.

5. It is observed that the increase of concrete strength is indirectly proportional with ductility and causes deterioration on the column ductility after yielding of steel tube.

6. Using high strength steel tube section in CFT columns can eliminate the post-peak softening behavior observed in columns subjected to high axial load, or columns with large concrete compressive strength and D/t ratio.

7. Using high strength concrete with high diameter to thickness ratio columns must be avoided to sustain ductility of composite columns.

REFERENCES

1. Sakino. K, Nakahara, H., Morino, S., Nishiyama, I., "Behavior of Centrally Loaded Concrete-Filled Steel-Tube Short Columns", *Journal of Structural Engineering,ASCE*, Vol.3, No.130, pp.180-188, February 2004.

2. Hu, H. T., Huang, C.S., Chen, Z.L., "Finite element analysis of CFT columns subjected to an axial compressive force and bending moment in combination", *Journal of Constructional Steel Research*, No. 61,pp. 1692–1712, 2005.

3. Fujimoto, T.; Mukai, A.; Nishiyama, I.; Sakino, K., "Behavior of Eccentrically Loaded Concrete-Filled Steel Tubular Columns", *Journal of Structural Engineering,ASCE*, Vol. 130, No. 2, pp.203-212,February 2004.

4. Spacone, E. and El-Tawil, S.,"Nonlinear Analysis of Steel-Concrete Composite Structures:State of the Art", *Journal of Structural Engineering,ASCE,* Vol. 130, No. 2, pp.159-168, February 2004.

5. Hajjar, J. F., "A distributed plasticity model for concrete-filled steel tube beam columns with interlayer slip", *Engineering Structures,* Vol. 20, No. 8, pp. 663-676, 1998.

6. Dundar,C., Tokgoz,S., Tanrikulu,A.K., Baran,T., "Behavior of reinforced and concrete-encased composite columns subjected to biaxial bending and axial load", *Building and Environment,ELSEVIER,* 2007.

7. Roeder, C. W., Cameron, B., and Brown. C. B., "Composite Action in Concrete Filled Tubes", *Journal of Structural Engineering,ASCE,* Vol. 125, No. 5, pp. 474-484, May, 1999.

8. Hajjar, J. F. and Gourley, B. C., "Represantation of Concrete-Filled Steel Tube Cross Section Strength", *Journal of Structural Engineering,ASCE,* Vol. 122, No. 11, pp. 1327-1336, November 1999.

9. Lakshmi, B. and Shanmugam N. E., "Nonlinear Analysis of In-Filled Steel-Concrete Composite Columns", *Journal of Structural Engineering,ASCE*, Vol. 128, No. 7, pp.922-933, July 2002.

10. Ellobody, E., Young, B., Lam, D., "Behavior of normal and high strength concrete-filled compact steel tube circular stub columns", *Journal of Constructional Steel Research,* Vol. 62,pp. 706–715, 2006.

11. Liang,Q.Q, Uy, B:, J.Y. R., Liew, "Nonlinear analysis of concrete-filled thin-walled steel box columns with local buckling effects", *Journal of Constructional Steel Research*, Vol. 62,pp. 581–591, 2006.

12. Drucker, D. C. and Prager, W., "Soild mechanics and plastic analysis for limit design", *Quarterly of Applied Mathematics*, vol. 10, no. 2, pp. 157-165, 1952.

13. Inai, E.; Mukai, A.; Kai, M.; Tokinoya, H.; Fukumoto, T.; Mori, K.,"Behavior of Concrete-Filled Steel Tube Beam Columns", *Journal of Structural Engineering,ASCE*, Vol. 130, No. 2, pp.189-202,February 2004.

14. Hatzigeorgiou, G.D., "Numerical model for the behavior and capacity of circular CFT columns,Part I: Theory", *Engineering Structures,*(2007),in press

15. Huang C. S. et al., "Axial Load Behavior of Stiffened Concrete-Filled Steel Columns", *Journal of Structural Engineering,ASCE,* Vol. 128, No. 9, pp. 1222-1230, September 2002.

16. Abedi K., "A novel steel section for concrete-filled tubular columns", *Thin-Walled Structures,* No. 46, pp. 310–319, 2008.

17. Liew, J.Y. R. and Shanmugam, N.E., *"Theory and Analysis of Structures",* CRC Press LLC, 2003.

18. Mander, J.B., Priestly M.J.N., Park, K., "Theoretical Stress-Strain Model for Confined Concrete", *Journal of Structural Engineering, ASCE*, Vol.8, No.114, pp.1804-1849,1988

19. Ersoy, U. and Özcebe, G., (1995), "*Betonarme Yapıların Tasarımı*", Evrim Yayınevi, İstanbul.

20. Gourley, B. C., Tort C., Denavit, M.D., Schiller, P. H., Hajjar, J. F., "A Synopsis of Studies of the Monotonic and Cyclic Behavior of Concrete-Filled Steel Tube Members, Connections, and Frames", *NSEL Report Series,* Report No. NSEL-008,April 2008.

APPENDIX A: MATLAB CODE FOR FSA PROGRAM

```
%%%%%%%%%%%%%%%%%%%%%%%%%%%%%%%%%%%%%%%%%%%%%%%%%%%%%%%%%%%%%%%%%%%%%%%%%%%%
%                                                                           %
%                  FIBER STRESS ANALYSIS PROGRAM                            %
%                                                                           %
%                              FOR                                          %
%                                                                           %
%            CONCRETE FILLED TUBULAR(CFT)STEEL COLUMNS                      %
%                                                                           %
%%%%%%%%%%%%%%%%%%%%%%%%%%%%%%%%%%%%%%%%%%%%%%%%%%%%%%%%%%%%%%%%%%%%%%%%%%%%
%                                                                           %
% ** This computer program gives the data points of any circular CFT        %
% steel column by utilizing Sakino's material model to obtain moment –      %
% curvature diagram.                                                        %
%                                                                           %
%%%%%%%%%%%%%%%%%%%%%%%%%%%%%%%%%%%%%%%%%%%%%%%%%%%%%%%%%%%%%%%%%%%%%%%%%%%%
%                                                                           %
%ATTENTION: All measurement dimensions are in mm-stress are MPa- units,     %
%            except Loads, which are in kN. unit.                           %
%                                                                           %
%%%%%%%%%%%%%%%%%%%%%%%%%%%%%%%%%%%%%%%%%%%%%%%%%%%%%%%%%%%%%%%%%%%%%%%%%%%%


%%%%%%%%%%%%%%%%%%%%%%%%%%%%%%%INPUTS%%%%%%%%%%%%%%%%%%%%%%%%%%%%%%%%%%%%%%%%

D=222; %inner radius of steel tube
t=6.47; %thickness of steel
sigmas=835; %yield strength of steel
sigmac=77.6; %yield strength of concrete
sigmast=879; %Tensile strength of steel
STRN_su=0.101;%tensile strain of steel
F=4421;%Applied load
n=10; %No. of fiber in a half portion of section
Es=218000; %Elastic Modulus of Steel

%%%%%%%%%%%%%%%%%%%%%%%%%%%%%%%%%%%%%%%%%%%%%%%%%%%%%%%%%%%%%%%%%%%%%%%%%%%%
%%%%%%%%%%%%%%%%%%%%%%%%%%% GEOMETRIC PARAMETERS %%%%%%%%%%%%%%%%%%%%%%%%%%%
%%%%%%%%%%%%%%%%%%%%%%%%%%%%%%%%%%%%%%%%%%%%%%%%%%%%%%%%%%%%%%%%%%%%%%%%%%%%

R=D/2;
r=R-t; %Radius of column
Dc=D-2*t; %Radius of concrete
finc=R/n; %fiber thickness

%%%%%%%%%%%%%%%%%%%%%%%%%%%%%%%%%%%%%%%%%%%%%%%%%%%%%%%%%%%%%%%%%%%%%%%%%%%%
%%%%%%%%%%%%%%%%%%%%%%%%% MATERIAL MODEL PARAMETERS%%%%%%%%%%%%%%%%%%%%%%%%%%
%%%%%%%%%%%%%%%%%%%%%%%%%%%%%%%%%%%%%%%%%%%%%%%%%%%%%%%%%%%%%%%%%%%%%%%%%%%%

%%%(SAKINO'S CONCRETE MODEL)
gamau=1.67*Dc^-0.112; %scale effect coefficient
sigmacp=gamau*sigmac;%strength of plain concrete reduced by strenth
factor
sigmar=-(2*t*(-0.19)*sigmas)/(D-2*t); %radial pressure at steel
```

```
sigmare=0.17826*sigmar; %confining pressure on the concrete
Ec=(6.9+3.32*sigmacp^0.5)*10^3;%Elastic modulus of concrete
STRNco=0.94*sigmacp^0.25*10^-3;%strain at ultimate strength of unconfined
concrete
K=1-4.1*(2*t/(D-2*t))*(-0.19*sigmas/sigmacp);
sigmaccB=sigmacp+4.1*sigmar; %stregtn of confined concrete
if K<=1.5 %"if": STRNcco, STRNcco=strain at ultimate strength of confined
concrete
    STRNcco=STRNco+4.7*STRNco*(K-1);
else
    STRNcco=3.4*STRNco+20*STRNco*(K-1);
end
V=Ec*STRNcco/sigmaccB;
W=1.5-(17.1*10^-3)*sigmacp+2.39*sigmare^0.5;

%%%(STEEL MODEL)
STRN_sy=sigmas/Es;%Strain of steel at yielding point
STRNPC=0.91*STRN_sy;%Strain of steel at yielding point under compression
STRNPT=1.08*STRN_sy;%Strain of steel at yielding point under tension
Et=(sigmast-sigmas)/(STRN_su-STRN_sy); %second modulus of steel


%%%%%%%%%%%%%%%%%%%%%%%%%%%%%%%%%%%%%%%%%%%%%%%%%%%%%%%%%%%%%%%%%%%%%%%%%%%%
%%%%%%%%%%%%%%%%%%CALCULATION OF FIBER PROPERTIES%%%%%%%%%%%%%%%%%%%%%%%%%%
%%%%%%%%%%%%%%%%%%%%%%%%%%%%%%%%%%%%%%%%%%%%%%%%%%%%%%%%%%%%%%%%%%%%%%%%%%%%

s=R; %Inital value of "s" must be equated to "R"
ARCSUM=0;
ARSSUM=0;

for i=1:1:n
    s=s-finc; %distance between center-line and bottom edge of the fiber
    alphain=acosd(s/r); %inner angle
    alphaout=acosd(s/R); %outer angle
    ARC(i)=pi*r^2*(2*alphain/360)-r^2*sind(2*alphain)*0.5-ARCSUM;%area of
concrete part in fiber i
    ARS(i)=pi*R^2*(2*alphaout/360)-R^2*sind(2*alphaout)*0.5-ARC(i)-
ARSSUM-ARCSUM;%area of steel part in fiber i
    ARCSUM=ARC(i)+ARCSUM;
    ARSSUM=ARS(i)+ARSSUM;
    p(i)=s+0.5*finc; %Distance between mid-point of the fiber and CL
end

fprintf('     M        CURVATURE\n   ');
fprintf('-------    ----------\n\n ');

for STRN=0.000001:0.0005:0.1
    FST=0;%stored internal force
    MST=0;%stored internal moment
    CURVST=0;%stored curvature
    for  c=0.4*R:-0.1:-R %"for": N.A. position
        FSUM=0;

%%%%%%%%%%%%%%%%%%%%%%%%%%%%%%%%%%%%%%%%%%%%%%%%%%%%%%%%%%%%%%%%%%%%%%%%%%%%
%%%%%%%%%%%%%%%%  CALCULATION OF FIBER STRESSES %%%%%%%%%%%%%%%%%%
%%%%%%%%%%%%%%%%%%%%%%%%%%%%%%%%%%%%%%%%%%%%%%%%%%%%%%%%%%%%%%%%%%%%%%%%%%%%
```

```
        for i=1:1:n %"for": stress calculation of fibers for concrete and
steel parts
            mup=p(i)-c; %Distance between mid-point of the top fiber and
NA.
            mdown=-p(i)-c; %Distance between mid-point of the bottom
fiber and NA.

            STRNUP=abs(mup/(R-c))*STRN; %Top fiber strain
            STRNDOWN=abs(mdown/(R-c))*STRN; %Bottom fiber strain

            %%Determination of fiber stresses for concrete and steel
element
            if mup>=0 %case for upper fiber
                STRSCUP=CSTRSC(V,W,sigmaccB,STRNUP,STRNcco); %Compression
stress of concrete
                STRSSUP=CSTRSS(sigmas,STRNUP,STRNPC,Et,Es); %Compression
stress of steel
            else
                STRSCUP=0; %Tension stress of concrete
                STRSSUP=-TSTRSS(sigmas,STRNUP,STRNPT,Et,Es); %Tension
stress of steel
            end

            if mdown>=0 %case for down fiber
                STRSCDOWN=CSTRSC(V,W,sigmaccB,STRNDOWN,STRNcco);
%Compression stress of concrete
                STRSSDOWN=CSTRSS(sigmas,STRNDOWN,STRNPC,Et,Es);
%Compression stress of steel
            else
                STRSCDOWN=0; %Tension stress of concrete
                STRSSDOWN=-TSTRSS(sigmas,STRNDOWN,STRNPT,Et,Es); %Tension
stress of steel
            end

%%%%%%%%%%%%%%%%%%%%%%%%%%%%%%%%%%%%%%%%%%%%%%%%%%%%%%%%%%%%%%%%%%%%%%%
%%%%%%%%%%%%%%CALCULATION OF FIBER ELEMENT FORCES%%%%%%%%%%%%%%
%%%%%%%%%%%%%%%%%%%%%%%%%%%%%%%%%%%%%%%%%%%%%%%%%%%%%%%%%%%%%%%%%%%%%%%
            FCUP=ARC(i)*STRSCUP/1000; % Concrete force of upper fiber
            FSUP=ARS(i)*STRSSUP/1000; % Steel force of upper fiber
            FUP=FCUP+FSUP; % Total force of upper fiber
            FCDOWN=ARC(i)*STRSCDOWN/1000;% Concrete force of down fiber
            FSDOWN=ARS(i)*STRSSDOWN/1000;% Steel force of down fiber
            FDOWN=FCDOWN+FSDOWN; % Total force of down fiber
            FSUM=FSUM+FDOWN+FUP;% Total load carried by section
        end %"end": stress calculation of fibers for concrete and steel
parts

        DELTAP=abs((FSUM-F)/F);%Difference between internal&external
loads
        if ((FSUM>0 && DELTAP<=0.001))% "if": Check for equilibrium
equations
            FSUM=0;
            MSUM=0;
            for i=1:1:n
                mup=p(i)-c; %Distance between mid-point of the top fiber
and NA.
                mdown=-p(i)-c; %Distance between mid-point of the bottom
fiber and NA.
                STRNUP=abs(mup/(R-c))*STRN; %Top fiber strain
```

```
                STRNDOWN=abs(mdown/(R-c))*STRN; %Bottom fiber strain

                %%Determination of fiber stresses for concrete and steel
element
                if mup>=0 %case for upper fiber
                    STRSCUP=CSTRSC(V,W,sigmaccB,STRNUP,STRNcco);
%Compression stress of concrete
                    STRSSUP=CSTRSS(sigmas,STRNUP,STRNPC,Et,Es);
%Compression stress of steel
                else
                    STRSCUP=0; %Tension stress of concrete
                    STRSSUP=-TSTRSS(sigmas,STRNUP,STRNPT,Et,Es); %Tension
stress of steel
                end

                if mdown>=0 %case for down fiber
                    STRSCDOWN=CSTRSC(V,W,sigmaccB,STRNDOWN,STRNcco);
%Compression stress of concrete
                    STRSSDOWN=CSTRSS(sigmas,STRNDOWN,STRNPC,Et,Es);
%Compression stress of steel
                else
                    STRSCDOWN=0; %Tension stress of concrete
                    STRSSDOWN=-TSTRSS(sigmas,STRNDOWN,STRNPT,Et,Es);
%Tension stress of steel
                end

%%%%%%%%%%%%%%%%%%%%%%%%%%%%%%%%%%%%%%%%%%%%%%%%%%%%%%%%%%%%%%%%%%%%%%%%%%%%
%%%%%%%%%%%%%CALCULATION OF FIBER ELEMENT FORCES%%%%%%%%%%%%%%%%%%%%%%%%%%%%
%%%%%%%%%%%%%%%%%%%%%%%%%%%%%%%%%%%%%%%%%%%%%%%%%%%%%%%%%%%%%%%%%%%%%%%%%%%%
                FCUP=ARC(i)*STRSCUP/1000; % Concrete force of upper fiber
                FSUP=ARS(i)*STRSSUP/1000; % Steel force of upper fiber
                FUP=FCUP+FSUP; % Total force of upper fiber

                FCDOWN=ARC(i)*STRSCDOWN/1000;% Concrete force of down
fiber
                FSDOWN=ARS(i)*STRSSDOWN/1000;% Steel force of down fiber
                FDOWN=FCDOWN+FSDOWN; % Total force of down fiber

                MUP=FUP*p(i)/1000;  %Moment of up fiber wrt CL
                MDOWN=FDOWN*-p(i)/1000; %Moment of down fiber wrt CL

                FSUM=FSUM+FDOWN+FUP;%Total load carried by section
                MSUM=MSUM+MUP+MDOWN;%Total moment carried by section
            end
            CURV=STRN/(R-c)*100*D; % Curvature of section
            if MSUM>=MST
                MST=MSUM;
                CURVST=CURV;
                FST=FSUM;
                cst=c;
            end
        end %end: Check for equilibrium equations

    end %end: c
    if ((FST>0))
        fprintf('   %5.2f     %8.4f\n ',MST,CURVST);
    end
end % end:STRN
```

```
%%%%%%%%%%%%%%%%%%%%%%%%%%%%%%%%%%%%%%%%%%%%%%%%%%%%%%%%%%%%%%%%%%%%%%%%%%%%
%                                                                              %
% ** Function CSTRSSC="Compressive Stress of Concrete"                         %
%    based on Sakino's concrete model for circular CFT columns.                %
%                                                                              %
%%%%%%%%%%%%%%%%%%%%%%%%%%%%%%%%%%%%%%%%%%%%%%%%%%%%%%%%%%%%%%%%%%%%%%%%%%%%

function STRSC=CSTRSC(V,W,sigmaccB,STRN,STRNcco)
X=STRN/STRNcco;

STRSC=(V*X+(W-1)*X^2)*sigmaccB/(1+(V-2)*X+W*X^2);



%%%%%%%%%%%%%%%%%%%%%%%%%%%%%%%%%%%%%%%%%%%%%%%%%%%%%%%%%%%%%%%%%%%%%%%%%%%%
%                                                                              %
% ** Function CSTRSSS="Compressive Stress of Steel"                           %
%                                                                              %
%%%%%%%%%%%%%%%%%%%%%%%%%%%%%%%%%%%%%%%%%%%%%%%%%%%%%%%%%%%%%%%%%%%%%%%%%%%%

function STRSS=CSTRSS(sigmas,STRN,STRNPC,Et,Es)
if STRN<=STRNPC
    STRSS=Es*STRN;
else
    STRSS=0.91*sigmas+(STRN-STRNPC)*Et;
end

%%%%%%%%%%%%%%%%%%%%%%%%%%%%%%%%%%%%%%%%%%%%%%%%%%%%%%%%%%%%%%%%%%%%%%%%%%%%
%                                                                              %
% ** Function TSTRSSS="Tensile Stress of Steel"                               %
%                                                                              %
%%%%%%%%%%%%%%%%%%%%%%%%%%%%%%%%%%%%%%%%%%%%%%%%%%%%%%%%%%%%%%%%%%%%%%%%%%%%

function STRSS=TSTRSS(sigmas,STRN,STRNPT,Et,Es)
if STRN<=STRNPT
    STRSS=Es*STRN;
else
    STRSS=1.08*sigmas+(STRN-STRNPT)*Et;
end
```

APPENDIX B: FSA OUTPUTS FOR ANALYZED SPECIMENS

- **SPECIMEN: EC4-A-4-035**

M	CURVATURE
10.54	0.1197
26.03	0.5690
28.63	1.0554
29.07	1.3523
29.14	1.4516
29.18	1.5486
29.22	1.6466
29.02	2.6937
28.98	2.7860
28.94	2.8782
28.90	2.9705
28.86	3.0627
28.82	3.1550
28.79	3.2472
28.55	3.7914
28.51	3.8834
28.36	4.2411
28.33	4.3329
28.20	4.6886
28.17	4.7802
28.14	4.8718
27.99	5.3167
27.93	5.4860
27.90	5.5772
27.85	5.7455
27.80	5.9129
27.75	6.0796
27.68	6.3357
27.63	6.5006
27.56	6.7545
27.52	6.9176
27.47	7.0799
27.43	7.2414
27.42	7.3306

- **SPECIMEN: EC4-A-4-06**

M	CURVATURE
14.68	0.2870
16.88	0.3624
18.76	0.4372
22.70	0.6533
24.03	0.7977
24.41	0.8707
24.70	0.9450
24.88	1.0169
25.02	1.0897
25.10	1.1632
25.14	1.2353
25.17	1.3785
25.17	1.4494
25.11	1.5205
25.06	1.5919
24.90	1.7324
24.67	1.9421
24.57	2.0110
24.48	2.0799
24.39	2.1488
24.30	2.2176
24.01	2.4198
23.80	2.5526
23.73	2.6212
23.53	2.7534
23.34	2.8851
23.10	3.0846
22.92	3.2153
22.74	3.3454
22.57	3.4751
22.53	3.5430
22.36	3.6721
22.19	3.8007
22.15	3.8683
22.00	3.9964
21.95	4.0639
21.80	4.1914
21.76	4.2588
21.62	4.3857
21.58	4.4529
21.48	4.5121
21.45	4.5792
21.41	4.6464
21.28	4.7721
21.25	4.8391
21.12	4.9643
21.09	5.0312
21.00	5.0890
20.99	5.1558
20.89	5.2800
20.79	5.4037
20.70	5.5270
20.61	5.6499
20.52	5.7723
20.44	5.8943
20.36	6.0158
20.28	6.1370
20.20	6.2577
20.13	6.3780
20.06	6.4323
20.06	6.4978
19.99	6.5519

- **SPECIMEN: EC4-C-8-045**

M	CURVATURE
119.55	0.2255
149.95	0.3148
172.47	0.4051
189.55	0.4936
200.82	0.5835
206.99	0.6738
210.28	0.7642
211.74	0.8545
211.85	0.9423
211.32	1.0291
209.95	1.1140
208.19	1.1975
206.07	1.2789
203.75	1.3593
201.38	1.4399
198.65	1.5174
195.88	1.5947
193.14	1.6719
190.28	1.7471
187.29	1.8201
184.54	1.8946
181.69	1.9667
178.72	2.0363
175.99	2.1074
173.14	2.1759
170.36	2.2439
167.65	2.3112
165.01	2.3780
162.26	2.4419
159.61	2.5050
157.04	2.5676
154.42	2.6269
151.84	2.6828
149.26	2.7461
146.66	2.8088
144.41	2.8739
141.92	2.9357
139.47	2.9971
137.37	3.0609
135.03	3.1214
132.75	3.1814
130.81	3.2440
128.65	3.3031
126.55	3.3618
124.52	3.4201
122.32	3.4746
120.37	3.5286
118.16	3.5754
115.98	3.6183
113.46	3.6606
111.65	3.7191
109.86	3.7774
108.11	3.8353
106.39	3.8929
104.36	3.9467
102.72	4.0036
101.12	4.0603
99.44	4.1166
97.79	4.1726
96.19	4.2284
94.63	4.2838
93.12	4.3390
91.53	4.3899
89.80	4.4366
88.21	4.4829

86.38	4.5209
84.36	4.5466
82.34	4.5837
81.15	4.6401
79.55	4.6923
78.39	4.7483
76.82	4.8000
75.69	4.8556
74.16	4.9068
73.07	4.9619
71.59	5.0127
70.54	5.0674
69.13	5.1176
68.14	5.1720
66.82	5.2218
65.46	5.2669
64.28	5.3161
63.18	5.3651
61.87	5.4094
60.70	5.4534
59.24	5.4881
57.45	5.5045
55.62	5.5206
54.55	5.5721
53.48	5.6235
52.41	5.6747
51.33	5.7257
50.26	5.7766
49.19	5.8273
48.13	5.8779
47.08	5.9283
46.52	5.9833
45.49	6.0334
44.47	6.0833
43.48	6.1331

- **SPECIMEN: EC4-C-8-06**

M	CURVATURE
126.42	0.3229
144.55	0.4015
157.06	0.4786
165.17	0.5531
170.73	0.6270
173.68	0.6985
171.49	0.9064
168.24	0.9723
164.66	1.0385
156.39	1.1667
151.66	1.2281
147.03	1.2894
142.53	1.3503
137.27	1.4080
117.61	1.6341
113.14	1.6894
107.98	1.7407
103.00	1.7914
98.21	1.8415
93.62	1.8909
83.94	1.9920
80.01	2.0438
75.20	2.0911
70.57	2.1378
66.12	2.1840
61.86	2.2296
56.98	2.2703
52.93	2.3148
48.91	2.3588
44.55	2.4023
39.92	2.4453
32.25	2.5346
28.06	2.5762
24.06	2.6174
20.25	2.6581
16.66	2.6984
12.55	2.7332
8.00	2.7626
4.56	2.8065
1.17	2.8500

- **SPECIMEN: EC4-D-4-04**

M	CURVATURE
217.50	0.2553
254.34	0.3312
279.46	0.4058
296.32	0.4788
307.62	0.5502
314.44	0.6203
318.38	0.6886
319.89	0.7552
317.64	0.8224
314.37	0.8887
310.18	0.9538
305.23	1.0185
299.59	1.0825
293.66	1.1455
287.55	1.2078
281.23	1.2692
274.91	1.3300
268.57	1.3902
262.43	1.4501
256.03	1.5089
249.82	1.5674
243.80	1.6251
237.59	1.6816
231.59	1.7376
225.58	1.7927
219.80	1.8474
214.03	1.9012
208.31	1.9540
202.65	2.0058
197.02	2.0582
192.02	2.1136
186.74	2.1676
181.43	2.2207
176.53	2.2741
171.76	2.3271
166.85	2.3792
162.08	2.4309
157.46	2.4824
153.00	2.5335
148.70	2.5843
144.34	2.6341
140.17	2.6835
135.99	2.7320
131.84	2.7793
127.69	2.8241
123.20	2.8620
119.05	2.9081
115.23	2.9576
111.44	3.0077
107.71	3.0575
104.38	3.1078
100.76	3.1572
97.55	3.2072
94.07	3.2561
90.98	3.3056
87.64	3.3541
84.70	3.4033
81.53	3.4514
78.46	3.4992
75.48	3.5469
72.60	3.5944
69.83	3.6416
66.98	3.6850
63.93	3.7255
60.72	3.7628
57.37	3.7962
54.09	3.8338

51.68	3.8813
48.98	3.9277
46.64	3.9748
44.01	4.0208
41.74	4.0677
39.51	4.1143
37.03	4.1599

- **SPECIMEN: EC4-D-4-06**

M	CURVATURE
225.96	0.2705
260.14	0.3462
282.95	0.4202
298.50	0.4927
308.99	0.5640
315.44	0.6340
318.99	0.7678
316.90	0.8354
313.27	0.9013
308.91	0.9661
304.03	1.0311
298.28	1.0948
291.76	1.1568
285.47	1.2186
279.39	1.2803
273.54	1.3418
266.79	1.4011
260.23	1.4601
253.86	1.5188
247.74	1.5772
242.03	1.6352
236.51	1.6929
230.12	1.7479
223.96	1.8025
218.02	1.8566
212.32	1.9102
206.86	1.9634
201.63	2.0162
195.65	2.0685
190.36	2.1233
185.50	2.1778
179.38	2.2290
174.80	2.2829
170.33	2.3364
165.99	2.3897
160.48	2.4395
156.41	2.4921
151.27	2.5412
147.49	2.5932
142.74	2.6416
139.28	2.6930
134.94	2.7406
130.85	2.7879
126.66	2.8312
121.51	2.8668
117.71	2.9165
113.66	2.9659
109.54	3.0151
107.25	3.0679
103.23	3.1167
99.29	3.1652
95.43	3.2135
93.31	3.2656
89.59	3.3134
85.98	3.3610
84.00	3.4126
80.55	3.4598
77.22	3.5068
74.00	3.5535
72.26	3.6044
69.28	3.6507
66.20	3.6923
62.56	3.7290
60.10	3.7700
56.58	3.8014
53.08	3.8417

49.71	3.8864
48.00	3.9355
44.73	3.9797
43.06	4.0286
41.41	4.0773
38.30	4.1210
36.72	4.1694
33.76	4.2128
32.26	4.2609
29.44	4.3039
27.12	4.3518
24.80	4.3995
22.49	4.4472
20.19	4.4947
18.16	4.5948
15.98	4.6421
14.41	4.6893
10.95	4.7308
9.45	4.7776
7.98	4.8244
6.52	4.8711
5.08	4.9176
1.93	4.9583
0.55	5.0046

- **SPECIMEN: EC6-A-4-02**

M	CURVATURE
42.09	1.9769
43.33	2.9537
43.86	3.6507
44.52	4.9367
44.96	6.1191
45.11	6.7436
45.31	7.5717
45.58	8.9011

- **SPECIMEN: EC6-A-4-06**

M	CURVATURE
20.26	0.5220
29.78	1.3818
31.81	1.7017
32.66	1.8992
33.57	2.1619
34.07	2.3638
35.69	3.2404
36.06	3.5821
36.47	3.9275
36.96	4.4733
37.19	4.8272
37.45	5.2513
37.45	5.3176
37.76	5.8800
38.14	6.7167
38.15	6.7837
38.69	8.2367

- **SPECIMEN: EC6-C-8-03**

M	CURVATURE
71.50	0.1768
205.07	0.8660
210.48	0.9646
223.20	1.4750
227.40	2.2816
227.00	2.9649
222.94	4.6755
221.33	5.3195
220.03	5.8642
218.66	6.4985
218.49	6.5925
216.93	7.4085
216.79	7.5021
215.35	8.4046

- **SPECIMEN: EC6-C-8-06**

M	CURVATURE
109.80	0.3786
122.44	0.4574
141.66	0.6117
149.04	0.6872
155.51	0.7623
161.02	0.8357
176.37	1.1186
178.85	1.1868
181.39	1.2555
183.88	1.3939
185.29	1.5999
184.95	1.7370
184.55	1.8748
184.03	1.9413
176.44	2.8055
175.90	2.8720
175.38	2.9385
173.20	3.1292
172.79	3.1955
171.17	3.3189
170.80	3.3850
168.89	3.5735
167.07	3.7609
165.33	3.9473
163.65	4.1326
162.05	4.3170
160.51	4.5004
159.02	4.6827
158.83	4.7476
157.62	4.8641
156.62	4.9800
156.50	5.0445
154.90	5.2239
153.20	5.4665
153.11	5.5307
151.53	5.7078
151.44	5.7718
149.79	6.0117
149.72	6.0755
148.09	6.3139
148.02	6.3776
146.35	6.6780
146.29	6.7415
144.64	7.0402
144.59	7.1035

- **SPECIMEN: EC6-D-4-03**

M	CURVATURE
177.10	0.1976
249.27	0.3024
309.83	0.4070
350.19	0.5038
454.82	0.9669
467.60	1.1619
472.01	1.2591
475.22	1.3578
484.78	1.9469
486.06	2.3321
486.07	2.5237
485.62	2.9023
485.42	2.9953
483.90	3.4694
483.52	3.5627
481.58	4.0290
481.19	4.1223
480.81	4.2155
478.41	4.7628
478.06	4.8558
475.86	5.4000
473.86	5.9414
473.58	6.0339
471.80	6.5723
470.18	7.1079

- **SPECIMEN: EC6-D-4-06**

M	CURVATURE
223.61	0.3239
251.96	0.4019
274.28	0.4784
292.81	0.5538
321.01	0.7012
332.40	0.7732
342.27	0.8440
357.97	0.9824
364.46	1.0508
374.83	1.1848
386.48	1.5185
387.86	1.5869
388.03	1.6525
387.89	1.7869
387.09	1.8526
386.65	1.9876
385.95	2.0534
385.29	2.1192
384.65	2.1850
381.69	2.3781
380.85	2.4438
379.78	2.5095
378.74	2.5752
377.73	2.6409
376.80	2.7066
375.99	2.7723
373.48	2.8984
372.75	2.9639
370.36	3.0895
369.70	3.1549
368.05	3.2145
367.42	3.2799
365.21	3.4043
364.65	3.4696
363.06	3.5284
362.53	3.5935
360.97	3.6520
360.47	3.7170
358.46	3.8400
358.00	3.9049
356.49	3.9626
356.07	4.0273
354.58	4.0847
354.17	4.1494
352.32	4.2710
351.95	4.3355
349.01	4.5209
348.79	4.5853
346.60	4.7057
346.39	4.7700
344.22	4.8898
344.03	4.9540
341.88	5.0733
341.70	5.1374
339.40	5.3201
339.25	5.3840
336.98	5.5660
334.75	5.7473
334.62	5.8110
332.41	5.9915
332.29	6.0551
330.02	6.2984
329.91	6.3619
327.78	6.5408
327.68	6.6042
327.59	6.6676

325.49	6.8457
325.41	6.9090
325.33	6.9722
323.27	7.1495

- **SPECIMEN: EC8-A-4-015**

M	CURVATURE
7.79	0.1243
13.83	0.2256
19.78	0.3287
52.94	1.1571
54.15	1.2408
55.67	1.4178
59.37	2.2418
60.24	2.6063
60.67	2.8932
60.8	2.988
61.06	3.1786
61.19	3.2744
61.56	3.5576
62.07	4.0386
62.14	4.1369
62.36	4.4341
62.87	5.2144
63.04	5.5022
63.58	6.5472
63.94	7.4121

- **SPECIMEN: EC8-A-4-06**

M	CURVATURE
24.09	0.4763
25.83	0.5519
27.28	0.6254
28.50	0.6971
29.63	0.7681
30.58	0.8371
31.56	0.9070
32.40	0.9753
33.23	1.0436
33.95	1.1105
34.72	1.1782
36.00	1.3098
37.16	1.4400
37.76	1.5055
38.89	1.6356
39.41	1.7000
39.82	1.7625
41.18	1.9523
41.58	2.0148
41.98	2.0774
42.38	2.1400
42.77	2.2025
43.17	2.2651
43.56	2.3277
44.68	2.5810
44.94	2.6467
45.09	2.7094
45.35	2.7753
45.50	2.8381
45.77	2.9043
45.92	2.9672
46.35	3.0965
46.49	3.1594
47.23	3.4152
47.37	3.4782
47.52	3.5412
48.16	3.8698
48.29	3.9376
48.41	4.0056
48.70	4.2056
48.86	4.3378
49.01	4.4066
49.18	4.5393
49.36	4.6723
49.55	4.8057
49.77	5.0033
49.96	5.1374
50.18	5.3359
50.37	5.4706
50.40	5.5348
50.64	5.7343
50.67	5.7986
50.88	5.9342
50.91	5.9986
50.97	6.0629
51.02	6.1273
51.12	6.1990
51.13	6.2635
51.20	6.3355
51.26	6.4077
51.27	6.4722
51.33	6.5447
51.40	6.6173
51.41	6.6820
51.48	6.7549
51.49	6.8197

51.56	6.8928
51.57	6.9577
51.64	7.0310
51.65	7.0960

- **SPECIMEN: EC8-C-8-06**

M	CURVATURE
123.83	0.5128
132.70	0.5867
140.71	0.6593
148.01	0.7319
154.54	0.8030
160.69	0.8737
166.22	0.9439
171.58	1.0139
176.84	1.0838
181.66	1.1526
186.11	1.2206
190.44	1.2887
194.61	1.3569
198.46	1.4243
202.20	1.4915
205.82	1.5583
209.25	1.6247
212.77	1.6914
215.72	1.7566
219.06	1.8229
222.11	1.8886
224.85	1.9533
227.61	2.0182
230.48	2.0832
232.98	2.1472
235.49	2.2112
237.58	2.2740
239.90	2.3408
241.45	2.4078
243.04	2.4751
244.65	2.5426
246.31	2.6103
247.68	2.6767
249.07	2.7432
250.49	2.8100
251.93	2.8768
253.39	2.9439
254.40	3.0128
255.14	3.0801
256.16	3.1495
257.22	3.2191
258.02	3.2870
258.84	3.3551
259.69	3.4233
260.60	3.4917
261.52	3.5603
262.13	3.6269
262.96	3.6957
263.79	3.7647
264.39	3.8316
264.99	3.8986
265.85	3.9680
266.35	4.0375
266.79	4.1073
267.42	4.1796
267.87	4.2497
268.34	4.3199
268.81	4.3903
269.29	4.4609
269.59	4.5290
270.08	4.5999
270.59	4.6709
270.90	4.7393
271.42	4.8107
271.74	4.8793
272.06	4.9480

272.38	5.0167
272.94	5.0886
273.27	5.1576
273.61	5.2266
273.96	5.2958
274.30	5.3650
274.66	5.4343
275.01	5.5037
275.13	5.5698
275.49	5.6394
275.86	5.7089
276.23	5.7786
276.34	5.8449
276.71	5.9182
276.87	5.9882
277.02	6.0582
277.36	6.1319
277.52	6.2022
277.69	6.2725
277.85	6.3429
278.02	6.4133
278.20	6.4839
278.38	6.5545
278.56	6.6253
278.74	6.6961
278.93	6.7670
279.12	6.8380
279.32	6.9090
279.51	6.9802
279.72	7.0514

- **SPECIMEN: EC8-C-8-07**

M	CURVATURE
120.23	0.7593
125.54	0.8273
130.57	0.8948
135.43	0.9621
139.90	1.0284
144.03	1.0948
148.03	1.1610
151.79	1.2266
155.45	1.2921
158.97	1.3572
162.28	1.4217
165.54	1.4862
168.48	1.5506
171.58	1.6155
174.28	1.6793
177.10	1.7436
179.74	1.8074
182.16	1.8706
184.67	1.9341
186.97	1.9969
189.39	2.0600
191.51	2.1223
193.67	2.1847
195.50	2.2461
197.36	2.3077
199.66	2.3706
201.17	2.4312
203.12	2.4932
205.11	2.5553
206.67	2.6161
208.25	2.6770
209.84	2.7379
211.45	2.7989
213.07	2.8600
214.70	2.9212
215.83	2.9808
217.56	3.0437
218.38	3.1067
219.29	3.1698
220.24	3.2331
221.20	3.2966
222.19	3.3601
222.85	3.4220
223.87	3.4858
224.55	3.5478
225.62	3.6118
226.33	3.6740
227.05	3.7363
227.77	3.7986
228.51	3.8610
229.26	3.9234
230.02	3.9860
230.37	4.0464
231.14	4.1090
231.93	4.1717
232.53	4.2345
232.83	4.2973
233.46	4.3626
233.99	4.4280
234.24	4.4911
234.74	4.5568
235.25	4.6226
235.52	4.6860
236.06	4.7520
236.34	4.8156

236.63	4.8792
237.20	4.9457
237.50	5.0095
237.81	5.0734
238.13	5.1373
238.45	5.2013
238.78	5.2654
239.11	5.3296
239.45	5.3938
239.79	5.4581
240.15	5.5225
240.50	5.5870
240.55	5.6484
240.92	5.7129
241.29	5.7775
241.67	5.8422
241.73	5.9037
242.12	5.9685
242.51	6.0334
242.58	6.0950
242.98	6.1599
243.05	6.2215
243.46	6.2866
243.54	6.3483
243.96	6.4135
244.18	6.4787
244.32	6.5441
244.46	6.6095
244.61	6.6750
244.76	6.7405
244.91	6.8061
245.07	6.8718
245.24	6.9376
245.40	7.0035
245.33	7.0655
245.50	7.1314
245.68	7.1974
245.86	7.2635
246.05	7.3297

- **SPECIMEN: EC8-D-4-015**

M	CURVATURE
121.55	0.1387
197.20	0.2439
269.90	0.3517
341.10	0.4600
411.04	0.5682
479.82	0.6758
599.50	0.9563
620.65	1.0512
648.60	1.2479
667.32	1.4493
674.21	1.5508
685.69	1.7593
690.45	1.8634
694.66	1.9662
697.86	2.0731
700.94	2.1785
703.94	2.2846
706.85	2.3901
711.43	2.6060
713.45	2.7152
715.36	2.8234
720.42	3.1406
721.88	3.2471
725.26	3.5753
726.33	3.6836
727.37	3.7922
728.37	3.9013
729.37	4.0083
733.09	4.4389
733.95	4.5472
735.42	4.7646
736.64	4.9862
737.25	5.0959
737.83	5.2059
738.39	5.3162
738.94	5.4267
740.04	5.6451
741.07	5.8643
743.04	6.3013
743.51	6.4100
745.32	6.8417
746.12	7.0560
747.27	7.3756

- **SPECIMEN: EC8-D-4-045**

M	CURVATURE
255.75	0.3307
325.50	0.4252
367.94	0.5121
398.83	0.5947
423.93	0.6754
445.79	0.7541
465.03	0.8311
482.32	0.9066
498.62	0.9817
513.25	1.0556
527.00	1.1288
540.17	1.2015
551.69	1.2724
563.13	1.3434
574.10	1.4140
584.52	1.4840
593.86	1.5527
602.03	1.6240
608.10	1.6975
614.23	1.7714
619.75	1.8440
625.30	1.9168
629.31	1.9923
633.02	2.0673
636.78	2.1426
640.30	2.2173
643.57	2.2912
647.15	2.3664
649.79	2.4429
652.17	2.5196
654.59	2.5968
656.81	2.6731
659.06	2.7496
661.08	2.8252
663.38	2.9023
665.44	2.9783
667.31	3.0532
668.91	3.1296
670.40	3.2076
671.70	3.2844
673.01	3.3615
674.34	3.4387
675.69	3.5161
676.81	3.5922
677.94	3.6684
679.08	3.7447
680.23	3.8212
681.39	3.8978
682.55	3.9745
683.45	4.0496
684.64	4.1266
685.55	4.2018
686.76	4.2790
687.62	4.3545
688.32	4.4319
689.03	4.5095
689.76	4.5872
690.49	4.6650
691.24	4.7430
691.74	4.8190
692.51	4.8972
693.03	4.9734
693.82	5.0519
694.39	5.1305
694.97	5.2092
695.55	5.2881

696.14	5.3671
696.73	5.4462
697.14	5.5231
697.74	5.6025
698.16	5.6795
698.77	5.7591
699.19	5.8363
699.81	5.9162
700.24	5.9936
700.67	6.0710
701.10	6.1485
701.54	6.2261
701.97	6.3037
702.41	6.3815
702.85	6.4592
703.29	6.5371
703.74	6.6150
704.19	6.6930
704.63	6.7710
705.09	6.8492
705.32	6.9243
705.78	7.0056
706.10	7.0871